Master's thesis
Faculty of Sciences
University of Bern

Co-occurrence of hail and rainfall

Handed in by
Stella Bērziņa

2023

Supervisor
Prof. Dr. O. Romppainen-Martius
Co-supervisor
Dr. C. Schwierz

Abstract

Hail is a common and costly natural hazard in Switzerland. The compound event of hail and rainfall can exacerbate the damage to property. Although there is literature on Eulerian hail and rainfall climatologies in Switzerland, when combined, they do not show the distribution of the compound hail-rainfall events. This is because hail and rainfall have to occur not only spatially but also temporally close to one another to create a compound event. Previous studies have not explored rainfall occurrence before and after a hail event from an Eulerian perspective in Switzerland.

This master's thesis explores the co-occurrence of hail and rainfall with a case study of 28 June 2021 and an analysis of the 2021 convective season. The case study results indicate that on 28 June 2021 hail and rainfall co-occurred in large areas of Switzerland. Moreover, in 88% of the co-occurrence area, hail and extreme rainfall (rainfall rate $\geq$ 24 mm/h) occurred within 10 minutes of each other, thereby creating a compound event. The close time proximity, the large impact area and the high cumulative amount of rainfall after the hail likely were the main contributors to the costly damages.

The convective season analysis showed that the cumulative amount of rainfall in the 6 hours after a hail event is significantly higher than in the 6 hours before the hail event. The rainfall accumulations are not homogeneous in the study area in space or time. South of the Alps, a streak of high accumulated rainfall values, especially before the hail, is observed around the Lago Maggiore region. This is likely linked to the convective echo trains explained in Panziera et al. (2015).

A larger estimated hail size in the 2021 convective season leads to a decrease in the accumulated rainfall before hail occurrence. This is attributed to the increased explosivity and translational speed of a hail storm, with increasing storm severity. Increased explosivity and translational speed lead to a smaller possible accumulation time of rainfall over an area.

The presence of a front in the proximity of the study area is found to have an impact on the cumulative rainfall amount associated with a hail event. In the north, the presence of a front leads to faster propagation speeds of the hail storms and, therefore, less accumulated rainfall. However, a typical synoptic situation (front entering from the west) south of the Alps leads to a southerly flow, and the storms tend to get orographically blocked. Therefore, in the south, no decrease in accumulated rainfall associated with fronts is observed, as fronts do not enhance the propagation speed of the storms in the way that they do in the north.

The main challenge of this topic is the large errors in radar rainfall estimates that arise from the presence of hail stones. The reliability and limitations of using 5-minute CombiPrecip (CPC) and Probability of Hail (POH) data are also explored in this thesis. Although it is possible to investigate hail and rainfall co-occurrence with the CPC and POH data sets, a wider ground hail sensor network would provide great help in validating the hail estimates that would improve our confidence in the data.

Contents

1 Introduction

Hail is one of the costliest natural hazard in Switzerland (Schemm et al., 2016; NCCS, 2021) and hail-related damages to infrastructure amount to approximately 93 million Swiss Francs annually (NCCS, 2021). The losses can be amplified if a hail event co-occurs with heavy rainfall and a compound event is created (Ridder et al., 2020). The definition of compound events by Ridder et al. (2020) states that the occurrence of both events will intensify the impacts, compared to individual events occurring in isolation. There are three main examples of hail and rainfall compound events : (1) if hail-induced debris (leaves, branches, hailstones) blocks water drainage systems and the subsequent rainfall causes flooding (Grahame et al., 2009), (2) if large hail occurs and damages buildings, especially roofs, co-occurrent heavy rainfall will lead to a flooding of the building (Hohl et al., 2002; Schuster et al., 2005), (3) if hail occurs without or before rainfall, cars tend to have increased damages (Pers. Comm. with O. Romppainen-Martius, 2023). Due to these costly damages, understanding the co-occurrence of hail and rainfall is of interest to both society and insurance companies.

1.1 Hail and rainfall observations

Hail is a low-probability high-impact event (Delobbe and Holleman, 2006) that is associated with high spatial variability (Sánchez et al., 2013). Therefore, to examine the co-occurrence of hail and rainfall, the precipitation data are needed with a high spatio-temporal resolution to capture the high variability.

In Switzerland, there is no extensive hail pad or sensor network, and hail sensors in chosen locations have been introduced only in recent years (Kopp et al., 2022). Additionally, compared to temperature or rainfall, observational networks need to be at least ten times denser to capture all hail streaks, because of their high spatial variability (Wieringa and Holleman, 2006). In spite of there being a large rain gauge measurement network in Switzerland, it is still not detailed enough in space to examine the co-occurrence of hail and rainfall. Therefore, the radar network is used to acquire considerably long-term, dense spatial coverage and high temporal resolution hail and rainfall data.

The radar network in Switzerland currently consists of 5 dual-polarisation radars (Figure 1), but in the last 10 years, the radar types and numbers have changed (Joss et al., 1998; Germann et al., 2015). Despite the fact that the radar network has changes in the past, it is possible to acquire good-quality radar data since 2002 (Nisi et al., 2016). Although radars provide high spatiotemporal resolution data, there are multiple challenges which affect the data quality, for example, partial beam blocking and beam shielding, which becomes especially prominent in the complex terrain of Switzerland (Germann et al., 2006; Joss et al., 1998). For a detailed discussion of the challenges of radar-based products, see Nisi et al. (2016) section 3.5.

Several studies have shown that using volumetric radar reflectivity produces reliable estimates of hail that reaches the ground (Kunz and Kugel, 2015). Additionally, radars have been named the most powerful remote sensing tools for the detection and size estimation of hail (Allen et al., 2020). However, there is no direct relationship between hail size or abundance on the ground and

the reflectivity observed by the radar. Therefore, hail stone size or amount cannot be directly inferred from the radar reflectivity and the results are only an estimate of hail occurrence (Allen et al., 2020). Because rain tends to not produce radar reflectivity values higher than 55 dBz, any reflectivity values exceeding this (and especially > 60 dBz) are an indicator of the presence of hail of any size (Allen et al., 2020).

It is essential to acknowledge that, due to the fact that hail and rainfall estimations are derived from the same radar reflectivity, it is hard to disentangle these signals, especially if both hail stones and raindrops are present in a cloud. The rainfall estimates can be "polluted" by the higher reflectivity of hail, which leads to higher estimated rainfall values than would be recorded if hail stones were not present. The error is reduced by correcting radar rainfall estimates with rain gauge data. However, hail is sparsely systematically observed on the ground, therefore, hail estimates are not ground-truth corrected. For more information on the challenges with radar hail and rainfall estimates see the Section 5.3.

Another way to validate radar estimates of hail (besides ground measurement network) is by using insurance damage data. Nisi et al. (2016) validated radar-derived hail estimates with vehicle hail loss data and found that the probability of hail (POH) $\geq 80\%$ is a good threshold to indicate hail occurrence. This threshold is widely used in the literature and this thesis (Section 3).

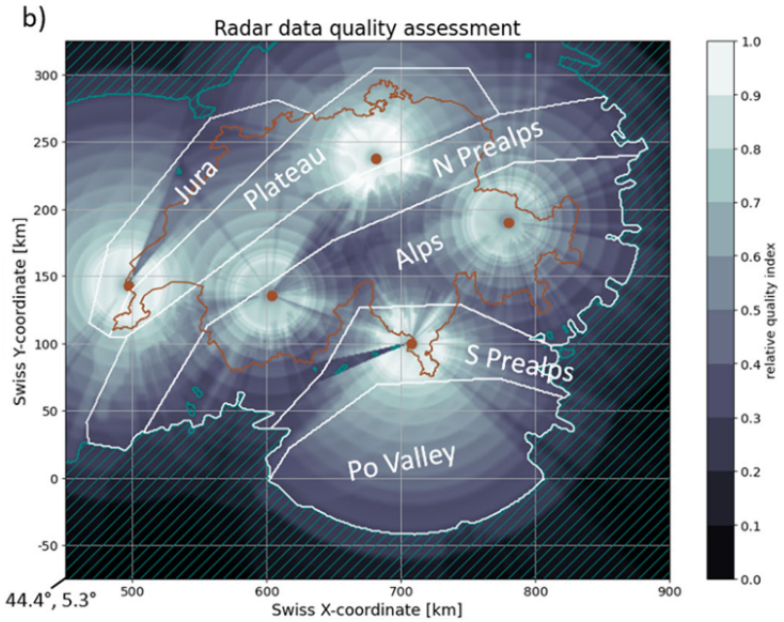

Figure 1: Relative data quality index of radar observations for convective phenomena (Feldmann et al. (2021)) and regional split with regions' names. Orange dots indicate the radar locations in Switzerland. The separation in 6 regions is not used in the analysis, but rather in the pattern description. Figure from Feldmann et al. (2023).

1.2 Hail and rainfall in Switzerland

There are two main paths that precipitation studies can take. The word "precipitation" in this thesis is used when referring to hail and rainfall together. First, one can explore the Lagrangian view in which the analysis follows an object, in this case, a convective storm. These studies usually deal

with the life cycle and along-track development of convective storms (Nisi et al., 2018; Feldmann et al., 2023). The other perspective looks at precipitation in fixed locations over time, called the Eulerian view. That is, the analysis is usually done on a per grid cell basis (Nisi et al., 2016; Barton et al., 2020). Therefore, the Eulerian view can more easily provide information that is related to the co-occurrence of hazards at a specific location, which this thesis aims to explore. The further section will provide information on studies on hail and rainfall in Switzerland.

1.2.1 Hail

In a convective storm, hail streaks (HST) are usually narrow and elongated areas within the storm path where hail occurs (Figure 2) (Nisi et al., 2018). One storm can create multiple HSTs (called hail swaths), but the majority of storms in Switzerland have only one HST (Nisi et al., 2018).

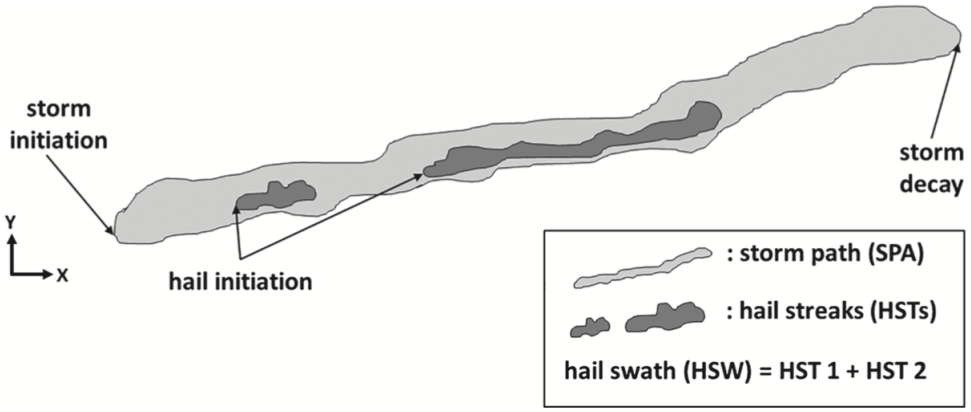

Figure 2: Illustration of storm path (SPA) and hail streaks (HSTs) in convective storms. Figure from Nisi et al. (2018).

The National Centre for Climate Services (NCCS) defines hail days as days with a high probability of hail (POH $\geq$ 80%) and reports that on average 33 hail days are observed in Switzerland from April to September (NCCS, 2021). Radar-derived hail day climatology shows the uneven spatial distribution with several maxima over the foothills north (Emmental, Entlebuch, and the Napf region) and south (Ticino) of the Alps and in the Jura region (Figure 3) (NCCS, 2021; Nisi et al., 2016). Hail hot spots suggest that orographic forcing is a key trigger for the formation and propagation of hail storms (and convection in general) because the instability can be easily released (Panziera et al., 2018; Nisi et al., 2018). The hot spots on average experience 2-4 hail events per season per square kilometre (Nisi et al., 2016). In contrast, in the inner-Alpine regions, convective storms are more rare (Figure 3), which can be explained by lower temperatures at higher elevations leading to reduced moisture content (Nisi et al., 2016).

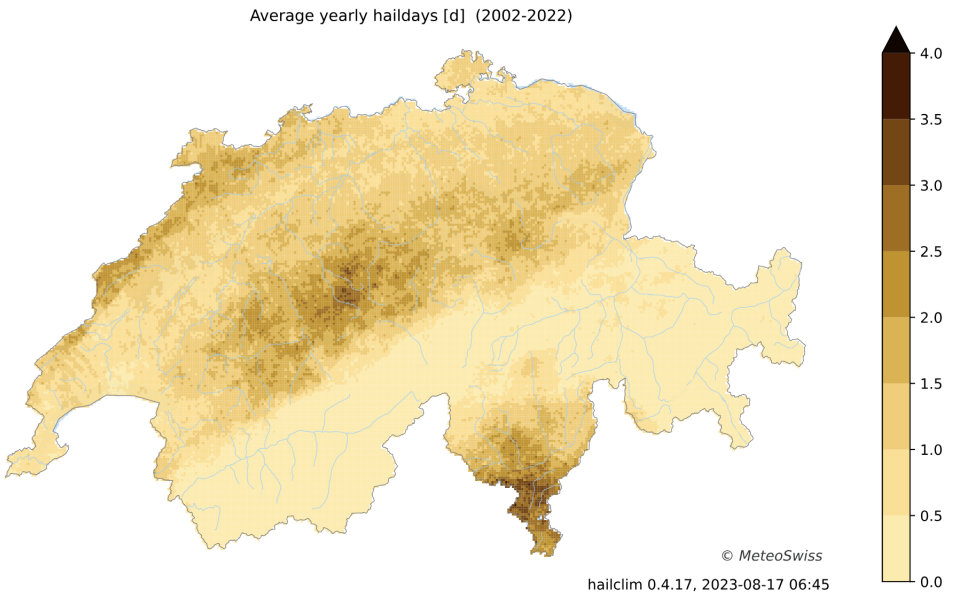

Figure 3: The mean annual number of hail days in Switzerland. Data 2002-2022 in 1 km^2 resolution. Figure from MeteoSwiss (2023).

Nisi et al. (2016) Eulerian climatology shows a seasonal and diurnal cycle in hail occurrence with peaks in July and late afternoons (1500 and 1700 UTC), respectively. In southern Switzerland on average hail occurs two hours later than in the north. Additionally, the southern regions experience larger hail (Nisi et al., 2016) and rainfall (Barton et al., 2020) occurrence time variability. That is, there is a less distinct peak in hail and rainfall occurrence time and precipitation tends to occur more evenly distributed during the day.

There is a gradient in precipitation occurrence times north of the Alps, with the Jura region showing the earliest hail occurrence peaks (1000-1400 UTC). It can be explained by the general flow patterns over Switzerland, whereby the largest fraction of fronts come from northwest and southwest (Jenkner et al., 2010). Nisi et al. (2018) showed that 62% of HSTs occur when westerly or southwesterly flow over Switzerland is present. During westerly flow HST frequency peaks around the Jura mountains in northern Switzerland. When SW flow is present, HSTs are more frequent in the southern Alps.

Depending on the location, 20-40% of hail events in Switzerland are associated with a front (Schemm et al., 2016). Especially at the start and end of the convective season (April-September), frontal lifting is needed as an additional force to trigger severe convection (Nisi et al., 2018; Schemm et al., 2016). Additionally, Schemm et al. (2016) found that the fraction of hail initiations related to fronts is highest in areas where hail is less frequent (especially in northern Switzerland). This suggests the hail maxima in the Prealps are more related to orographic forcing and airmass convection, which is probably more affected by differential heating and resulting thermal circulation as a triggering mechanism (Nisi et al., 2020).

Nisi et al. (2018) Lagrangian hail storm climatology showed that the size and longevity of the HST and storm path in general increase with increasing maximum estimated severe hail size (MESHS) within a storm (for more information on data see Section 2). Additionally, the Nisi et al. (2018) analysis shows that the more severe the hail storm (in terms of hail stone size produced),

the more explosive its development. This means that there is a shorter time and spatial difference between the first detection of a convective storm and HST initiation. The Lagrangian storm explosivity is 2.6-3.4 km or 10-25 minutes, depending on storm severity (Nisi et al., 2018). The HST initiation time and storm explosivity are relevant for the amount of rainfall that the area experiences before and after a hail event, especially if the storm is not fast-moving or is stationary.

Nisi et al. (2018) also showed a monthly cycle for the HST and storm paths. Storm path lengths have a minimum in June and July due to increased solar insulation and subsequent convection. On the other hand, HST are the longest from June to August. While storms persist longer in the colder shoulder months, Nisi et al. (2018) showed that moist and warm air masses are necessary for long-lived hail streaks.

In Nisi et al. (2018) the focus is on the hail initiation (information about the rainfall before a hail event) but little attention is paid to the decay of the storm and what happens after the hail event (rainfall after the hail event). Additionally, it is examined in Lagrangian view which is not ideal to analyse the likely impacts in specific areas.

The diurnal cycle of hail storm initiations and spatio-temporal development was explored in Nisi et al. (2020). They found that hailstorms that occur during the day will move towards higher elevations but the opposite is true for hailstorms that occur at night. This suggests the importance of Alpine pumping. Hail storms, compared to ordinary storms (without hail) are associated with higher vertical integrated liquid and vertical integrated liquid density (Nisi et al., 2020). This is likely due to the strong and persistent updrafts associated with hail storms. In these updrafts large amounts of humidity is added to the storm, thereby increasing the liquid water content.

Feldmann et al. (2023) looked into the differences in the life cycles and associated hazards in hail storms (MESHS $>$ 2cm), severe hail storms (MESHS $>$ 4cm), rain storms (hourly rainfall accumulation of $>$ 30mm/h) and severe rain storms ((hourly rainfall accumulation of $>$ 50mm/h) in Switzerland. The study found that 2/3 of hail and severe hail storms are also rain or severe rain storms, which is important for hail-rainfall compound events. The study also found that the translational speed of a storm increases with time, regardless of the storm class.

In summary, hail has a spatially varied occurrence frequency in Switzerland with hot spots in the Jura mountains, the northern and southern Prealps. Hail occurrence exhibits a diurnal cycle which is more pronounced north of the Alps. The time and location of hail occurrence is partly linked to the general flow patterns over Switzerland and the presence of fronts. The hail streak size and longevity within a storm varies depending on the month and the maximum estimated severe hail stone size. Lastly, the majority of hail storms also bring heavy rainfall.

1.2.2 Rainfall

Heavy and extreme rainfall, which have a more significant damage potential, can be considered on various accumulation time periods and the characteristics of the rainfall vary slightly on the time scale considered. For Switzerland, there are sub-hourly (5-minute) (Barton et al., 2020), extreme sub-daily (1-,6-,24-hour) (Panziera et al., 2018), and daily (Widmann and Schär, 1997) rainfall climatologies available. The general spatial patterns in all of these analyses are similar, whereby orography has a large impact on rainfall intensity and frequency with similar hot spots as seen

in Figure 3. Regardless of what heavy rainfall accumulation time scale is considered, Ticino in southern Switzerland is the most affected by heavy rainfall (Panziera et al., 2015; Barton et al., 2020).

Barton et al. (2020) assessed 5-minute precipitation characteristics, which are especially useful for investigating short convective events that are common in Switzerland in the warm months. The analysis showed that there is a distinct diurnal cycle of intensity (mean and extreme) and frequency in northern Switzerland with peaks in the Jura mountains occurring 2h earlier (1400-1700 UTC (corresponding to 1600 and 1900 local time)) compared to the Swiss Plateau (1800-2100 UTC) (Figure 4). This can also be linked to the previously discussed governing summer flow types, which are north- and south-westerly (Jenkner et al., 2010). In southern Switzerland, the 5-minute precipitation mean intensity and frequency are much more evenly distributed throughout the day without a distinct diurnal cycle (Figure 4). Additionally, in the south, the extremes are more frequent at night (2200 and 0100 UTC), which aligns with Nisi et al. (2016) hail observations.

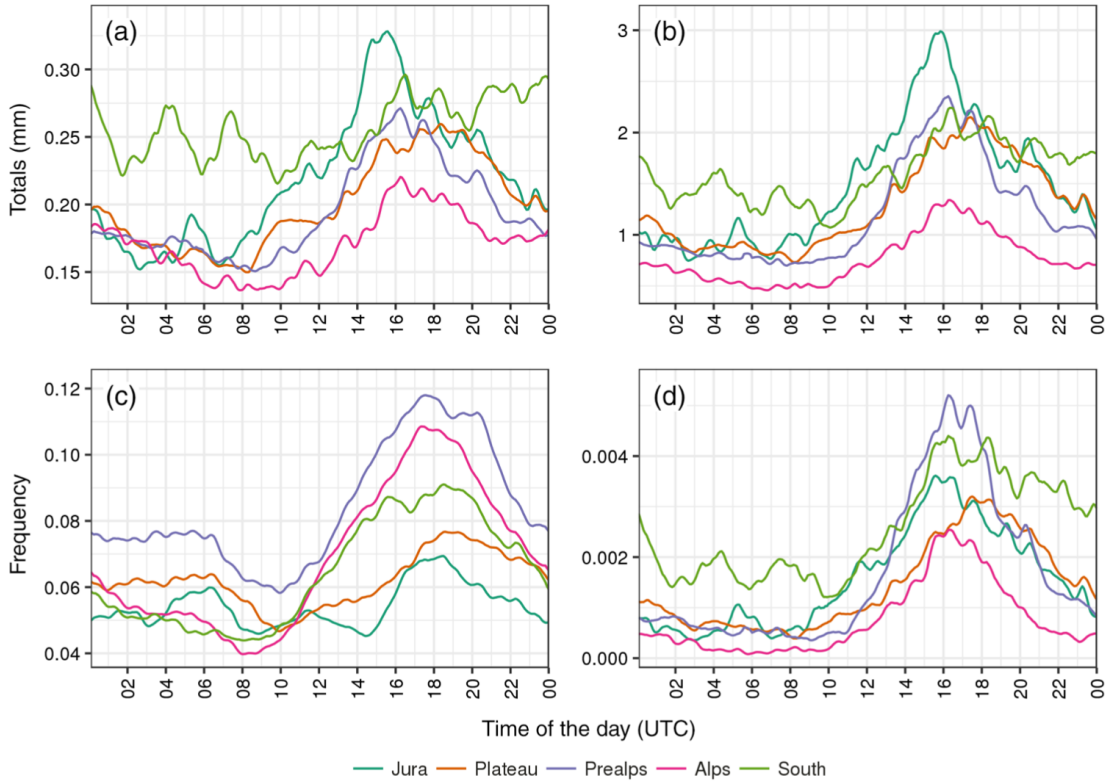

Figure 4: Diurnal cycle of 5-min (a) area-averaged mean wet totals and (b) area-averaged extreme totals, (c) mean wet frequencies and (d) extreme wet frequencies for summer. The colours indicate different regions in Switzerland. The time x-axis indicates the time of the day in UTC. The local time corresponds to UTC + 2. Figure from Barton et al. (2020).

Panziera et al. (2018) in detail explored 1-, 6- and 24-hour extreme rainfall in Switzerland by using the CombiPrecip (CPC) data set and compared the results to the Eulerian hail climatology of Nisi et al. (2016). The results showed similar general patterns of hail and extreme rainfall occurrence but slight differences on the local scales. For example, although the Lago Maggiore region is a hot spot for both hail and extreme rainfall, they have spatial distribution differences.

Hail is most often observed on the SE side of the lake in southern Ticino (Figure 3), but extreme rainfall peaks in a streak along the Lago Maggiore northern side (Figure 5).

Southern Switzerland, especially around the Lago Maggiore, is susceptible to flooding from intense rainfall although the rainfall frequency is relatively low (Isotta et al., 2014). Panziera et al. (2015) found that most intense flash flood events were associated with convective precipitation and echo training which arises when moist air from the Po Valley is advected to the Alps by a south-easterly low-level flow. After encountering the orography, the moist low-level air is lifted and convection is created. Then, the upper-level steering flow transports the convective cells to the northeast where they mature and dissipate. This model can describe elliptical high rainfall streaks that are observed in the region. The streaks described in Panziera et al. (2015) are visually similar to Figure 5 summer and autumn panels from Panziera et al. (2018) extreme rainfall study.

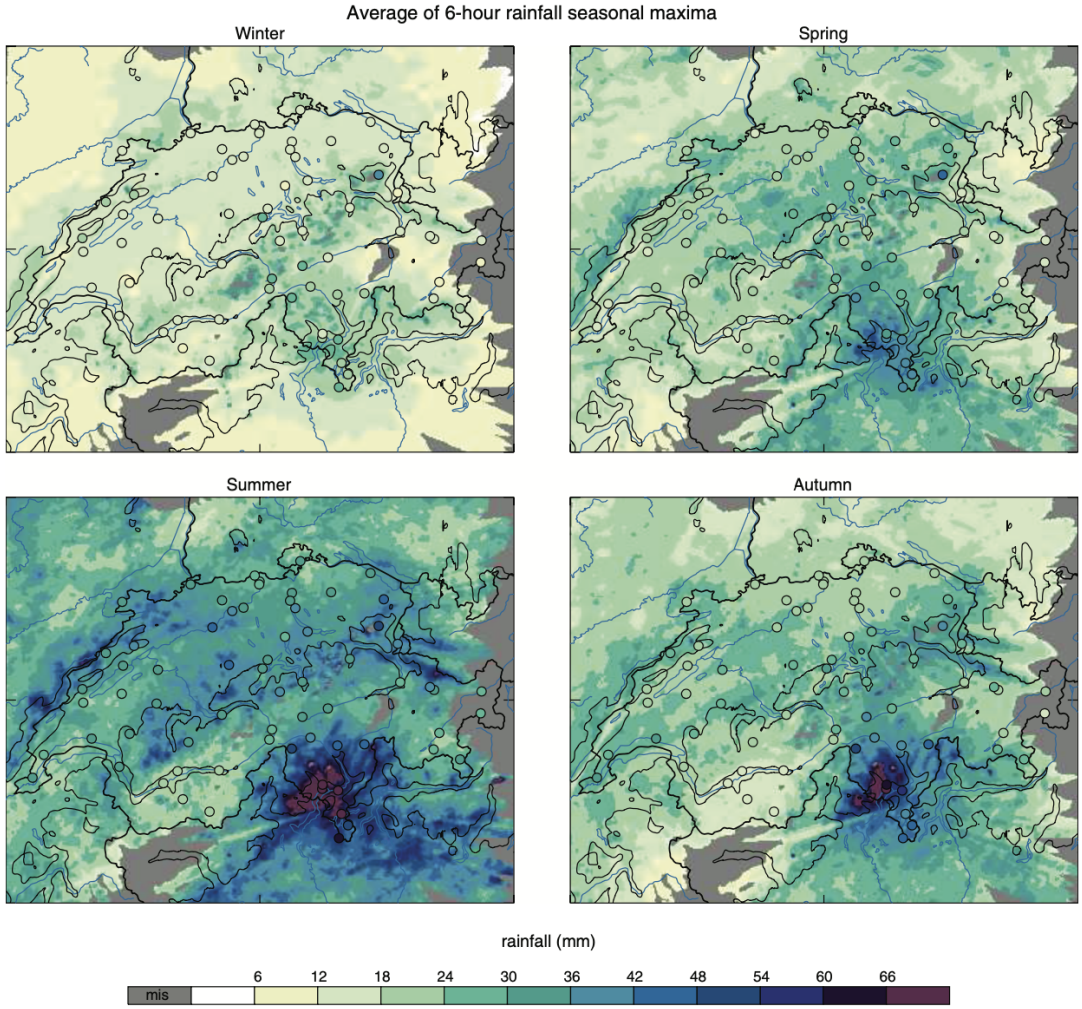

Figure 5: CPC average of 6-hr rainfall seasonal maxima. Small circles indicate the values of the rain gauges. The thick line indicates the borders of Switzerland, while the thin line denotes the 1,000 m a.s.l. orographic contour; the main lakes and rivers are drawn in blue Figure from Panziera et al. (2018).

Overall, the highest rainfall frequency and intensity is observed in the summer because of the increased convective activity (Panziera et al., 2018). However, in Ticino, the area with the heaviest

rainfall, maxima is observed during the autumn months and is linked to the large-scale circulation which during autumn tends to be southerly and therefore brings moist Mediterranean air toward the Alps (Panziera et al., 2018).

From a Lagrangian view, Feldmann et al. (2023) showed that rain storms and severe rain storms have a slower translational speed than hail-producing storms. This is important because it is the rainfall intensity and duration that contribute to the accumulation of rainfall in a given area. The more stationary the storm, the longer a given area will experience rainfall and accumulate more. Additionally Feldmann et al. (2023) shows that there is a linear increase in the storm speed, as it develops. This is attributed to the steering flow, which in the earlier development stages is closer to the ground and slower, but as the storm develops, it is steered more by the mid and upper-level flows. The longer the life cycle, the more acceleration the storm gets.

Aregger (2021) created a stationary convective storm climatology for Switzerland and only 3-4% of all convective storms were found to be stationary. The fraction of stationary storms is higher south of the Alps, when compared to the north. Northern parts are associated with a higher fraction of long track and long duration storms.

In summary, the hail and rainfall occurrence climatologies have similar spatial patterns but are not identical, especially in the southern Alps. There are seasonal and diurnal differences for mean and extreme rainfall, whereby northern and southern Switzerland exhibit different cycles. On shorter time scales (sub-daily) the precipitation maximum occurs in summer. The Lagrangian studies have touched on the rain and hail occurrence times in convective storms, however, it has not been explored in Eulerian perspective.

1.3 28 June 2021

On 28 June 2021 in the northern part of Switzerland, severe hail storms occurred. The storms affected the second-largest recorded area of severe (at least 100km^2 of MESHS $\geqslant$ 4cm) and extreme (at least 100km^2 of MESHS $\geqslant$ 6cm) hail north of the Alps in Switzerland (Kopp et al., 2022). Insurance companies reported record amounts of damage claims. For example, La Mobiliere reported 20,000 damage claims for vehicles and the building insurance company for the region of Lucerne (GVL) reported 18,000 damaged buildings after the hail events, which is six times more than the yearly average. The storms occurred in densely populated areas (e.g. Luzern, Zurich), so the day also experienced a peak of crowd-sourced hail reports in the MeteoSwiss application (Kopp et al., 2022).

At 1400 UTC storms originated in western Switzerland and moved eastward along the northern foothills of the Swiss Alps with multiple supercells and a mesoscale system being observed (Kopp et al., 2022). The storms persisted for multiple hours and covered large areas. The long lifetime of the mesoscale convective system combined with the path over densely populated areas were likely the main contributors to the large damages. Indeed, Schuster et al. (2005) indicated how important the location and orientation of the storm path is to the damages by a hail storm. Additionally, Hohl et al. (2002) reports that the highest insured losses in Switzerland occurred when hail moved over densely populated areas. Multiple news outlets reported on the storm and images and videos from the event time and the damages were widely shared on social media.

Hohl et al. (2002) reports on the hail storm that occurred on 5 July 1999. During the afternoon many hail cells crossed the canton of Bern as a part of a mesoscale convective system. Later, precipitation systems from France crossed the affected areas and produced rainfall that lasted overnight. The study concluded that the contributions to the damages of multiple convective cells are not proportionally additive. Rather, the loss increases dramatically with each consecutive cell crossing the same area. Similarly as on 28 June 2021, the rainfall following the hail caused major damage to the exposed internal building structures and basements, which would not have been damaged by the rainfall if the hail had not damaged the exterior of the building beforehand. The study reported that the occurrence of consecutive convective cells likely added to the total loss ratio (losses during the event/total insured value) that was 6 times higher than for other storms with similar hail intensity and size.

Figure 6: Hail stones on the case study day. (a) Hailstone A. Picture source: Sturmarchiv Schweiz/(www.sturmarchiv.ch, M. Kost, Wolhusen via SRF. (b) Hail damages in Wolhusen (location of hailstone A). Picture source: Sturmarchiv Schweiz/www.sturmarchiv.ch, Whatsapp, author unknown. (c) Hailstone B. Picture source: Sturmarchiv Schweiz/www.sturmarchiv.ch, Roland Müller, Nottwil via SRF. (d) Hailstones C. Picture source: SRF Meteo/https://twitter.com/srfmeteo/status/1413086126026461184, C. Brechbühl. (e) Hailstone D. Picture source: same as (d). Figure from Kopp et al. (2022).

1.4 Motivation and aim

Switzerland is regularly affected by severe hail storms causing substantial damage. Although there is literature on extreme rainfall and hail climatologies in Switzerland (subsection 1.2), the combination

of them does not explain hail-rainfall co-occurrence. This is because in order to have great impacts, hail and rainfall have to occur spatially and temporarily close to each other therefore creating a compound event. To the best of my knowledge, hail-rainfall co-occurrence in Switzerland from an Eulerian perspective has not been explored in the past. Given the impacts of the compound event, it is an important knowledge gap that needs to be further addressed in research. For example, the spatial disagreement between hail and extreme rainfall climatology hot spots in the southern Alps (Figures 3 and 5) will be interesting to explore in terms of the co-occurrence of hail and rainfall.

The co-occurrence of hail and rainfall in this study is explored from an Eulerian point of view. The Eulerian perspective provides information that is relevant to the impacts and damages, as it shows the co-occurrence on a per grid cell basis, rather than following the storm.

The main aim of this thesis is to investigate hail-rainfall co-occurrence in Switzerland in two parts. The **first part** is a case study of the damaging hail storms on 28 June 2021, which resulted in a record-breaking number of damage claims due to a combination of hail and flooding. In the case study, I will explore the sequence of occurrence of hail and extreme rainfall events. Additionally, the case study will be used as a "playground" to explore possible ways to look at the hail-rainfall co-occurrence and what uncertainties are associated with each of the results. This explorative analysis is further used as a basis for deciding what type of analysis to conduct in the second part of the thesis. The following questions about the specific study day will be answered:

1. In which areas did hail and rainfall co-occur and in what sequence?
2. What was the time difference between rainfall and hail occurrence? Did both come from the same convective system?
3. What is the cumulative rainfall amount before and after hail?

In the **second part** of the thesis, the whole convective season of 2021 will be analysed. The convective season analysis aims to quantify 6-hour cumulative rainfall before and after hail events. Additionally, it will be able to put into context the case study and see whether the cumulative rainfall amounts before and after the hail event on 28 June 2021 were unusually distributed or rather characteristic for the region. The following questions are addressed:

1. What is the typical rainfall distribution in the 6 hours before and after hail in the 2021 convective season?
2. Is there a difference between northern and southern Switzerland with regards to the characteristic rainfall amounts before and after hail?
3. Is there a monthly or diurnal difference in the cumulative rainfall amount before and after hail?
4. Is there a relationship between the cumulative rainfall before and after hail and the estimated (MESHS) hail stone size?
5. Does the presence of a front in the study area impact the cumulative rainfall before and after hail?

Additionally, as previously discussed, there is a lot of uncertainty associated with rainfall estimates that co-occur with hail. To try to validate the results, this thesis will also explore how much the hail signal distorts the rainfall estimates. This will be done by:

1. Comparison of the cumulative rainfall amount 6 hours after the start of the hail event and the cumulative 6-hour rainfall from the end of the hail event. This will test how robust are the results, and whether after the removal of the hail event from the cumulative rainfall the results still hold. If they do, that would indicate that even though we cannot fully trust rainfall estimates at the time of hail, this likely skewed estimate is not the only contributor to the cumulative sum.

2. Compare the results in the study area to the results only within the Swiss territory. This will show whether the differences, especially in the south of the Alps, arise from areas outside of Switzerland, where the CPC rainfall data is not corrected by rain gauges.

Another goal of this thesis is to explore whether POH and CPC data sets are the only data needed to look at the rainfall and hail occurrence in high resolution. There are other types of data that one can utilise, for example, crowdsourcing data (Barras et al., 2019), polarimetric data on hydrometer types (Besic et al., 2016), hail sensor measurements (Kopp et al., 2022) or insurance claims (Nisi et al., 2016). Each of the data sets comes with its own advantages and disadvantages. In this thesis, POH and CPC data sets are primarily used, as they are considered to have the highest sensitivity in Switzerland.

The structure of the thesis is as follows: Section 2 describes the data used in this study, followed by Section 3 on the methods used to answer the research questions. Section 4 contains the results which are discussed in the wider context of relevant literature in Section 5. Lastly, Section 6 summarises the main results and mentions the areas of possible future research.

2 Data

2.1 Study area

The study area was chosen to stretch 50 km outside the border of Switzerland (Figure 7) because these areas are still well covered by the Swiss radar network (Figure 1) and, therefore, offer a larger data set. For further analysis, the area is subdivided into northern and southern Alps (Figure 7 green and red areas) and the main Alpine chain is excluded from these areas because little to no hail occurs there (Nisi et al., 2016). In the Section 4.2.6 that explores the sensitivity of the results, the data only within the border of Switzerland is compared to the defined study area. The study area has a complex topography of the Alps and the terrain ranges 200-4000 masl.

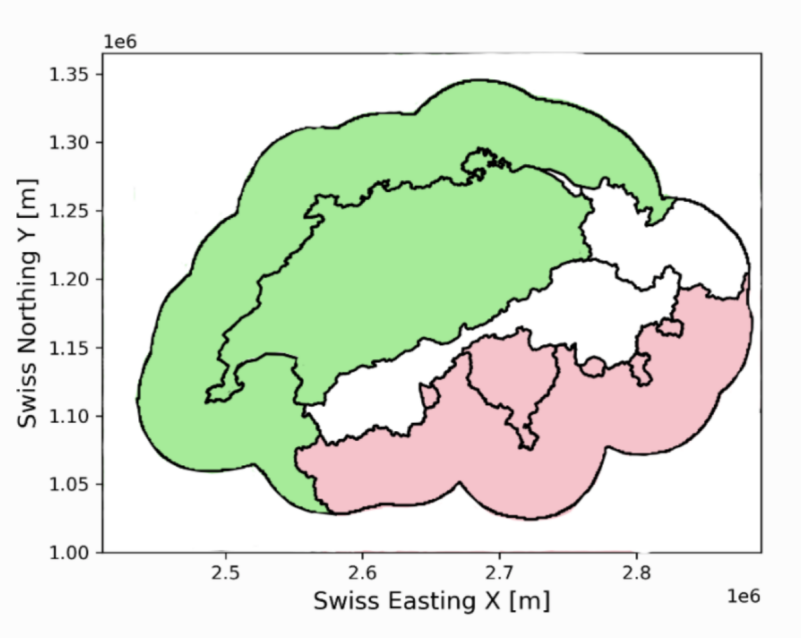

Figure 7: Study area. The whole study area is the smoothed outermost outline. It is further separated into the northern part in green (includes Jura, Plateau and Northern Prealps from Figure 1) and the southern part in red (includes Southern Prealps and the northern part of Po Valley from Figure 1). In the north/south division, the main Alpine chain region (in white) is excluded from the analysis. In subsection 4.2.6 the data within the Swiss borders is compared to the whole study area.

2.2 Radar Data

In this thesis, three types of radar data products are used and they are described below. All data sets are used in 5-minute temporal and 1 km^2 spatial resolution. Therefore, when a "grid cell" is discussed in the results, it refers to 1 km^2. The time steps used in this thesis are in UTC, not the local time in Switzerland (UTC + 2 hrs).

2.2.1 Rainfall data

MeteoSwiss uses the **CombiPrecip (CPC)** geostatistical merging to produce hourly estimates of rainfall rate on a 1x1 km resolution regular grid (Sideris et al. (2014)). CPC locally adjusts the radar rainfall map according to the values of the rain gauge measurements by using kriging.

For the purposes of this thesis, 5-minute CPC data is used because hail and rainfall have heterogeneous spatio-temporal occurrence. The 5-minute CPC data is created by redistributing the rain gauge corrected hourly rainfall value in the 5-minute intervals by taking into account only the radar 5-minute precipitation estimates (Barton et al., 2020). This means that the 5-minute CPC data carries the radar error in overestimation of rainfall, even if it technically is corrected by the rain gauge. Although hourly aggregations have the advantage of being more robust and stable (Sideris et al., 2014), Barton et al. (2020) showed that 5-minute disaggregation of the CPC data outperforms radar-only rainfall estimates in quantitative error values and the detection of wet/extreme periods.

An additional complication is that the rain gauge data that is used to correct the radar field comes only from the Swiss territory. The kriging between rain gauge measurements and radar estimates stretches a few tens of kilometres outside of the Swiss border and gradually fades into the radar estimate. It is important to keep this in mind, as the study area in this study spans outside of Swiss borders. The error associated with this is explored in Section 4.2.6 and in the discussion of the limitations of this thesis (Section 5.3).

Lastly, as mentioned previously, although the rainfall estimates are corrected, it is still not clear whether this eliminates the overestimation of rainfall when hail stones are present. Therefore, one must be cautious when analysing these results.

2.2.2 Hail data

Probability of hail reaching the ground (POH) is a radar data product that is operationally used by MeteoSwiss (Waldvogel et al., 1979; Foote et al., 2005). POH is an empirical hail detection algorithm and is based on the difference in height (Δz) between the altitude of the highest 45 dBZ echo and the height of the freezing level (H_0) which is retrieved from the forecasts of the numerical weather prediction model COSMO-1. For Δ z $<$ 1.65 km POH is 0%, while with Δ z $\geqslant$ 5.5 km it is 100%. POH has been validated using insurance loss data and the best overlap was found between hail damage and POH $\geqslant$ 80% (Nisi et al., 2016). Although Nisi et al. (2016) found that a POH threshold of 80% is relatively reliable, it is still possible that hail in a specific location occurs also if the POH value is lower than 80%. Moreover, it is possible that no hail occurs on the ground even if POH $\geqslant$ 80%. This uncertainty is associated with using radar-derived hail products that are not extensively validated with ground truth data.

The Maximum Expected Severe Hail Size (MESHS) algorithm (Treloar, 1998; Joe et al., 2004) is operationally used by MeteoSwiss and it estimates the maximum expected diameter of hail at the ground for hail $\geqslant$ 20 mm. MESHS is calculated with an algorithm that considers the highest altitude at which radar reflectivity of a minimum of 50 dBz can be detected and the H_0 from COSMO-1. MESHS has been validated in, for example, Nisi et al. (2016).

3 Methods

This chapter first explains which of the methods and definitions are used in the case study and the seasonal analysis. Because the case study is an exploratory part of the thesis, not all methods used in the case study are applied for the convective season analysis. On the other hand, some aspects that are not possible to explore on a single day, are explored in the seasonal analysis. Next, the methods and definitions used in this thesis are explained in separate subsections. Lastly, the statistical methods used in both parts of the thesis are explained in subsection 3.6.

Case study The case study is the first part of the thesis and its goal is to explore ways of quantifying hail and rainfall co-occurrence by investigating the convective events on 28 June 2021.

One of the aspects explored in the case study is the sequence of occurrence of hail and rainfall on the study day. For this, hail and rainfall thresholds are selected the definitions of hail and rainfall episodes (HE and RE) are introduced (subsections 3.1, 3.2). This allows for investigating the spatial and temporal co-occurrence of hail on rainfall on the case study day. Additionally, I am exploring the cumulative rainfall amount before and after the hail episode. The creation of the cumulative rainfall data set is explained in subsection 3.3 for the whole 2021 convective season. On the case study day, only the data between 0600 UTC 28 June and 0600 UTC 29 June from the cumulative rainfall dataset are analysed.

Convective season analysis After conducting the case study the analysis of the cumulative rainfall amount was chosen to investigate the 2021 convective season. This approach was selected because it does not involve defining a rainfall rate threshold, as a generally accepted definition of rainfall rate that can cause damage is lacking. The convective season in this thesis is defined from April to September.

For analysis of the cumulative rainfall before and after hail in the 2021 convective season, the definition of a hail episode is used (subsection 3.1). The further steps of creating the cumulative rainfall data set are explained in subsection 3.3. Finally, I also link the cumulative rainfall amounts to frontal activity (subsection 3.4) and stratify the results by hail episode severity (chapter 3.5).

3.1 Hail threshold and Hail episode (HE)

In the case study and the convective season analysis, the concept of a hail episode is used, which places more conditions than just POH$\geq$80% that need to be fulfilled to indicate the occurrence of hail in a grid cell.

A **hail episode (HE)** in a grid cell is defined as the occurrence of POH$\geq$80% at the same time step for 4 or more contiguous pixels (spatial continuity) for at least two time steps (10 minutes) (temporal continuity). Both spatial and temporal continuity conditions need to be fulfilled to create a HE.

The HE ends if either the spatial or temporal conditions are not fulfilled anymore for at least 30 minutes. If the HE conditions are fulfilled again after 30 minutes, this will be considered a new, separate HE. This means, that two HEs are separated by at least 30 minutes.

Using the HE definition sets a stricter threshold for hail occurrence area than just areas with POH≥80%. For example, in the case study, there is a reduction of the hail-affected area by 29% when the HE condition is set, compared to when only POH≥80% is used as a hail proxy.

In each grid cell where a HE occurs, all of the HE start and end times are recorded. The start of the HE is the first time step when the HE conditions are fulfilled. The end of a HE is determined by finding the first time step that has no instances of the HE definition being fulfilled in the following 30 minutes (6 time steps).

3.2 Rain episode (RE) and rainfall thresholds

Unlike the previously shown threshold for damaging hail, there is, to my knowledge, no universally accepted threshold for damaging rain. Here I use the CPC product and define the following thesholds:

1. A rainfall rate of 0.08 mm/h is the threshold used when considering minimum rainfall (including very light drizzle). This rainfall threshold is used to explore the co-occurrence of hail and any amount of rainfall. This rainfall rate is not associated with damages.

2. A threshold of 24 mm/h is used for extreme rainfall. It corresponds to the 99^{th} percentile of rainfall rate in Barton et al. (2020) over the most affected areas on the case study (northern Prealps and Plateau). However, in the south, the 99^{th} extreme rainfall rate is higher than the set threshold here (Barton et al. (2020)).

When other minimum or extreme rainfall rate thresholds are tested, the results are similar. So, although the threshold choice is arbitrary, the results are not very different if other thresholds are chosen.

The rainfall rate thresholds have units of mm/h, however, this rainfall rate has to occur only for one time step (5 minutes) to reach the threshold. It is possible that a grid point does not accumulate the threshold rainfall in an hour, as not all time steps within the hour (12 time steps) have the same rainfall rate. This means, that a 24 mm/h rainfall rate translates to a rainfall accumulation of 2 mm in 5 minutes.

An area experiences a **rain episode (RE)** if a rainfall rate of at least 24 mm/h is recorded in 4 or more neighbouring pixels for more than one time step. Similarly as for the HE definition, REs need to be separated by at least 30 minutes when the RE conditions are not fulfilled to count as separate episodes. In essence, REs refer to episodes of extreme rainfall on the case study day. The **co-occurrence area** is the area in which both HE and RE occur on the case study day. Rainfall thresholds, the RE and co-occurrence area definitions are used only in the case study.

3.3 Cumulative rainfall analysis

To create the 6-hour cumulative rainfall data set, first, for all the grid cells the HE start and end times are found. Next, from the CPC data, for all HEs a cumulative sum of rainfall is calculated for:

1. 6 hours before the HE (until the HE initiation time step)

2. 6 hours after the HE start (from the HE initiation time step)

3. 6 hours after the HE end (from the first time step when HE conditions are no longer fulfilled)

The values are stored in a data set, which contains approximately 73,000 individual hail episodes from the study area. Additionally, for each of the HEs, the 6-hour time series of rainfall rate before and after a HE is saved to explore the rainfall distribution around the HE (Section 5.2.2).

To explore the hail size and the cumulative rainfall, each entry also has the relevant MESHS value that was recorded in the grid cell at the time step when the HE started. The MESHS value at the HE initiation time is representative of the maximum estimated severe hail size recorded in the hail storm, as Feldmann et al. (2021) shows that MESHS values peak at the time when HE is initiated.

The large data set is further analysed by comparing the cumulative rainfall amounts pre- and post-HEs in various subgroups with the statistical methods noted in the Section 3.6:

1. Spatial separation (whole study area, northern and southern parts)

2. Temporal separation (monthly, hourly)

3. To explore likely dependencies:

   (a) MESHS size

   (b) Presence of a front

4. Area of Switzerland versus the study area to test the sensitivity of the results

3.4 Analysis of front data

The effect of fronts on the rainfall amount before and after a HE is examined. This is done by comparing HEs on days with fronts to days without. The front-day dataset was generated by using information from the UKMET synoptic chart archive (Wetter3.de, 2023). All days of the 2021 convective season are allocated into one of two groups- (1) no front present or (2) front present. The synoptic charts in the archive are available at 6-hour resolution, but in this thesis, the frontal information is aggregated to daily resolution. If at any of the 6-hour intervals during a day there is a front in the study area, then the day is marked as "front present". If a front is not present in any of the 6-hourly synoptic charts during a day, then the day is put into the "no front" group. I assume that if there is a front over the study area, then the hail episode that occurs on the day is related to the occurrence of the front. The division is done by visually assessing the location of the front on the synoptic map. A day is considered to exhibit a front if there is a front within approximately 200 km away from the study area, therefore, the days with fronts refer to frontal, pre-frontal and post-frontal environments. Schemm et al. (2016) found that on average in Switzerland the distance between the front line and the hail initiation area is approximately 200 km. As this is a visual assessment, the data set is associated with errors.

The analysis was also carried out by having more precise frontal categories, for example, front north or south of Alps. Later all groups were aggregated into one frontal group to (1) minimise

human error from the visual data assessment and (2) because results were similar in all frontal groups.

When all days of the convective season are allocated into two groups, the HEs are separated into groups according to the frontal situation on the day that the HE occurred. Next, these groups are analysed by the statistical methods listed in Section 3.6 to explore whether the HE of the days with a front have a different cumulative rainfall amount or distribution around a HE.

3.5 Storm-related definitions

There are terms that do not have a strict definition in the literature. In this section, I define what some of these terms mean in this thesis.

In this thesis, the possible link between cumulative rainfall around a HE and the hail severity is explored. For this, four thresholds are used to define hail size classes by using the MESHS data set: (1) [0-20 mm) (where a HE is detected but MESHS value is not present), (2) [20-40 mm), (3) [40-60 mm) (severe hail), (4) $\geq$60 mm (extreme hail). Therefore, in this thesis **hail severity** refers to only the size of the hail stone. **Storm severity** refers to the hail size recorded in a storm. Therefore, the hail and storm severity increases with the recorded hail size class.

Rain storm and hail storm in this thesis refers to the moving convective system that can be tracked by, for example, the thunderstorm radar tracking algorithm (TRT). This means, rain and hail storms lead to HEs and REs that occur in grid cells.

A universally agreed-upon definition of a time scale in which hail and rainfall have to co-occur to create a compound event is lacking. This is because the relevant time scales differ for the damages considered. In case of hail and other debris clogging the water drainage systems, shorter time scales are more relevant, as hail can stones melt. On the other hand, for the damaged roofs and subsequent flooding of the building, longer time scales of co-occurrence are more applicable. In this thesis, for a **compound event** the relevant time window within which hail and rainfall have to co-occur is 6 hours. Results of 4 to 7-hour accumulation times do not show major differences. The 6-hour window approximates the estimated time after which the occurrence of extreme rainfall will no longer greatly exacerbate the damages caused by hail. This is assuming that hail stones that would clog the drainage system have melted and that major external hail damage to buildings will be acknowledged and precautions are taken to reduce further water damage.

3.6 Statistical methods

3.6.1 Box plots

To visualise and easily compare the results of the cumulative rainfall before and after a HE, notched box plots are used. The box indicates 25% and 75% quartile range, line within the box is the median. The whiskers show 5% and 95% range. The figures in this thesis do not show outliers (values outside the whiskers).

Furthermore, to visually compare the box plots, notches are implemented. The notches provide a measure to determine the rough significance of differences between the medians in the box plots (McGill et al., 1978). The notches approximately indicate the the 95% confidence interval of the

median. If the notches around two medians do not overlap, the medians are roughly significantly different with alpha=0.05 McGill et al. (1978).

The formula for notches is derived empirically and is computed as

$$M \pm 1.7(1.25R/1.35\sqrt{N}) \tag{1}$$

Where **M** is the median, **R** is the interquartile range (a measure of spread) and **N** is the number of observations. In the cases when the confidence interval is above (below) the upper (lower) quartile, the notches extend beyond the box.

The notched box plot is not a statistical test, but rather a visual aid to show the differences in the distribution of the data. Additionally, the data groups that are visualised in a notched box plot (cumulative rainfall before and after the HE) are not strictly independent. Therefore, although the notches are an easy and convenient way of determining the significant differences, one has to be cautious in cases when the data is not fully independent, as the notches can overestimate the significant differences. Therefore a statistical test is carried out to help make a more reliable comparison of rainfall before and after a HE.

3.6.2 Wilcoxon Signed-Ranks Test

The Wilcoxon Signed Ranks Test is a non-parametric test that is viewed as the non-parametric alternative to the Student's t-Test for Matched Pairs. The Wilcoxon signed rank test was developed by Wilcoxon (1945).

The null hypothesis that is tested in the Wilcoxon signed-rank test is that the pairwise differences have a probability distribution centred at zero (Woolson, 2007). In this thesis the null hypothesis that is tested is that there is no difference in the distribution between:

1. 6-hour cumulative rainfall amount before a HE and 6-hour cumulative rainfall amount after the start of a HE
2. 6-hour cumulative rainfall amount before a HE and 6-hour cumulative rainfall amount after the end of a HE

The basic procedure of the Wilcoxon signed-rank test, as described in Woolson (2007), is:

1. Calculate the differences between the two samples and rank the absolute values disregarding any zeros
2. Compute the test statistic (**T**) by calculating the sum of the ranks of the positive and negative differences separately. The minimum of the sums is picked as the test statistic
3. Next, to test the null hypothesis, the test statistic must be compared to a distribution. For large samples, as in the current thesis, the standard normal distribution (**Z**) is used as an approximation

The distribution of **Z** is defined as:

$$Z = \frac{\frac{T - n(n+1)}{4}}{\sqrt{\frac{n(n+1)(2n+1)}{24}}} > Z_{1-\alpha/2} \tag{2}$$

where **n** is the number of observations and α is 0.05.

All of the test statistics and the associated p-values for each of the tests can be found in Appendix A.

4 Results

This section of the thesis presents the results of the case study (4.1) and the convective season analysis (4.2). When significant differences are mentioned, the relevant p-value and Wilcoxon test statistic can be found in Appendix A.

4.1 Case Study 28th June 2021

4.1.1 Hail and rain events

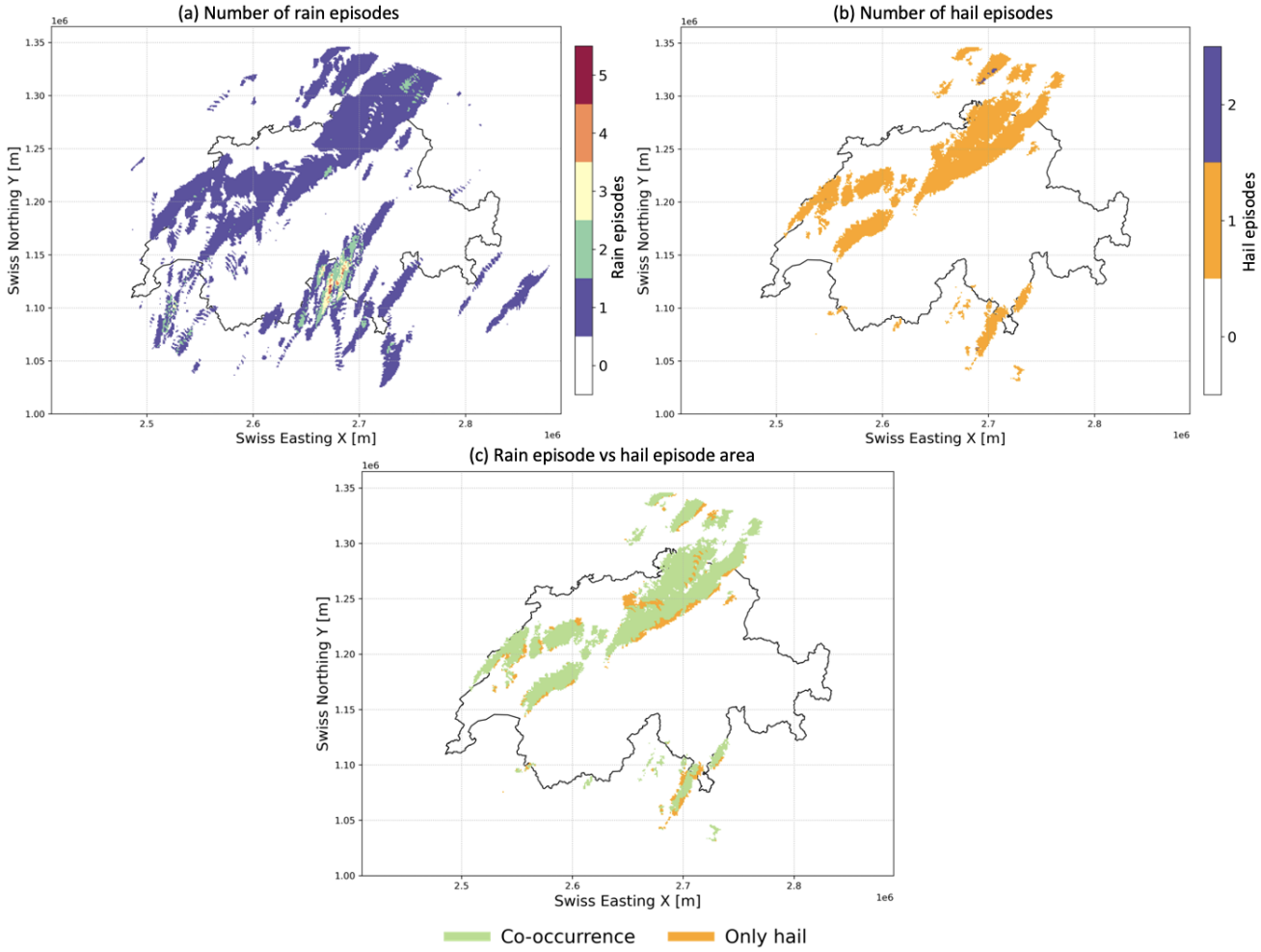

Figure 8: The affected area and the number of (a) rain episodes (rainfall rate $\geq$ 24 mm/h) and (b) hail episodes on 28 June 0600 to June 29th 0600, 2021.(c) shows the difference between (a) and (b) in orange indicating areas where hail occurred but not extreme rainfall episodes.

HEs and REs Figure 8 shows how many (a) rain episodes (REs) and (b) hail episodes (HEs) occurred in the study area on 28 June 2021. Over 92.8% of the area where a RE was recorded, only one RE occurred. 5.5% of the area had 2 REs, 1.4% had 3, 0.3% had 4 and only 7 grid cells (0.03%) had 5 REs. Most of the instances of multiple REs per grid cell occurred in the southern study area and the grid cells with a higher number of REs form an elongated streak pattern above the Lago Maggiore.

Figure 8 (b) shows that 99.6% of the area where a HE occurred, experienced only one HE, and 0.4% (38 grid cells) 2 HEs on the case study day. This allows us to assume that all of the study area experienced only one HE in further case study analysis.

Co-occurrence area All of the areas that experienced hail also experienced at least 0.08 mm/h rainfall (not shown). However, if an extreme rainfall threshold is considered, then 15.3% of the hail area did not experience a RE, as indicated in orange in Figure 8 (c). Therefore, in 84.7% of the area where hail occurred, also extreme rainfall occurred.

The majority of the hail-affected area is subjected to a likely hail-rainfall compound event due to the overlap of the areas of occurrence. To say whether there was a compound event, the occurrence times have to be compared, which is done in the following section.

4.1.2 Co-occurrence sequence

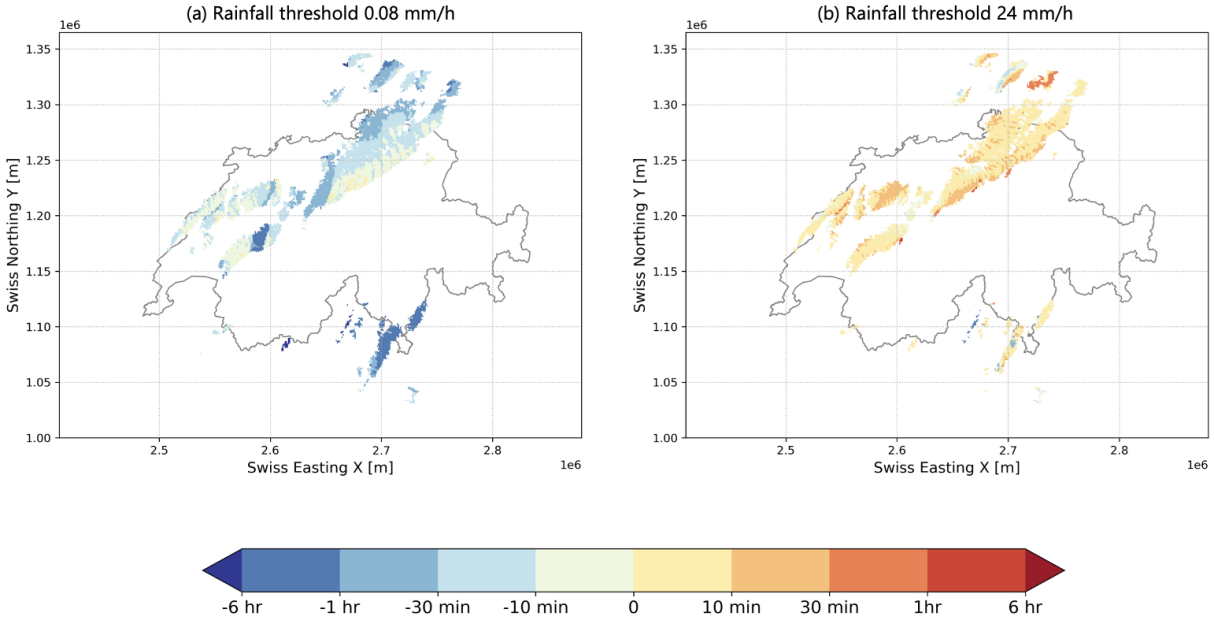

Figure 9: The time difference between the time step of hail episode initiation and the first time step with a rainfall rate of (a) 0.08 mm/h, (b) 24 mm/h. Blue colors indicate that rainfall occurred before hail, orange/red colors show that hail occurred before rainfall. The time steps that are compared in each grid cell are defined as follows: (1) For hail- the start time of the first HE on the case study day, (2) for minimum rainfall rate- the first time step when 0.08 mm/h is registered for at least one time step, (3) for extreme rain- the first time step of the first RE on the case study day.

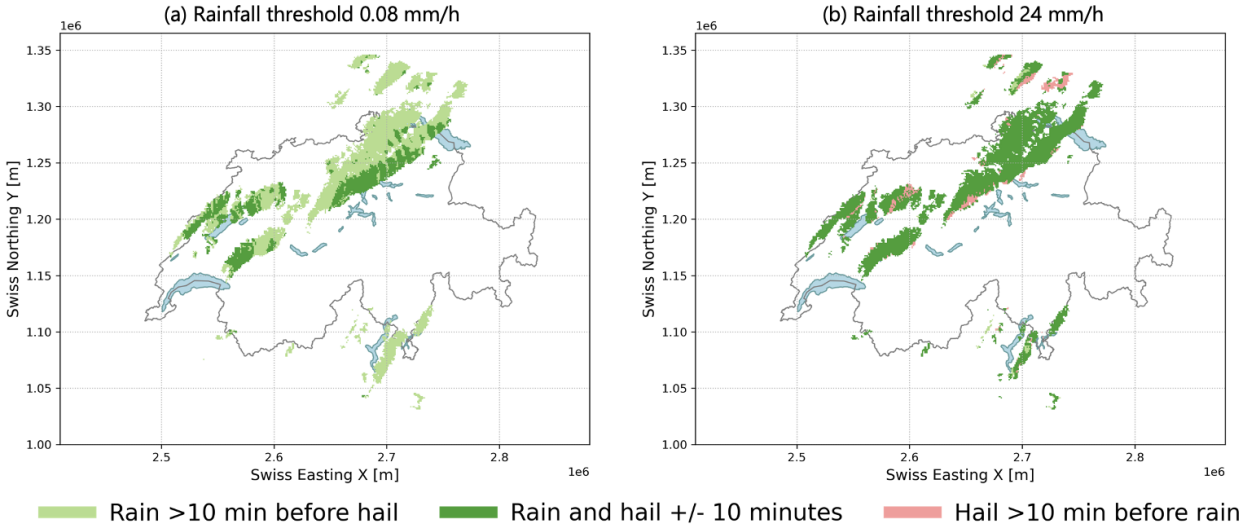

Figure 10: The sequence of occurrence of hail and rainfall rate of (a) 0.08 mm/h and (b) 24 mm/h. Similar to Figure 9 but grouped into 3 occurrence groups: (1) light green - rainfall more than 10 minutes before hail, (2) dark green - hail and rainfall within 10-minutes from each other, (3) pink - hail at least 10 minutes before rainfall. Only the time step of the first occurrence of hail or rainfall of the specific threshold is considered. Lakes indicated in light blue. The same time steps compared as described below Figure 9.

Figure 9 shows the temporal proximity and overlap of HEs and REs on the case study day by displaying the time difference between the rainfall (0.08 mm/h (a) and 24 mm/h (b)) and the HE occurrence. Figure 10 shows the same information as Figure 9 but it is divided into three groups that describe the occurrence sequence.

First, from Figure 9 it is visible that for both rainfall thresholds, the rainfall occurs within the +/- 1-hour window from a HE. Additionally, the time difference between HE and rainfall occurrence is varied over the study area.

When the threshold is 0.08 mm/h, the majority (78%) of the co-occurrence area first experience rainfall and only then hail, in 22% of the area it occurs at the +/- 10-minute time step and in no grid cells hail occurs before rainfall (Figure 10 (a)). Therefore, most areas where hail and rain co-occurred first experienced at least light drizzle before the HE.

In general, the lower the threshold, the larger the area that experiences rainfall before hail (Figure 10, Figure 9). Other rainfall rate values between 0.08 mm/h and 24 mm/h have been tested, but are not shown.

If the extreme rainfall occurrence (a RE) is considered (Figure 9 (b)), then it is less likely that an area will experience rain before hail. Only 4% of the co-occurrence area experiences extreme rainfall before hail (Figure 10 (b)). In 88% of the area, a RE occurs within the same 10-minute interval as the HE. In 8% of the area, a HE occurs more than 10 minutes before a RE. This indicates that the majority of the area experienced hail and extreme rainfall in a very close temporal proximity.

4.1.3 Cumulative rainfall before and after hail

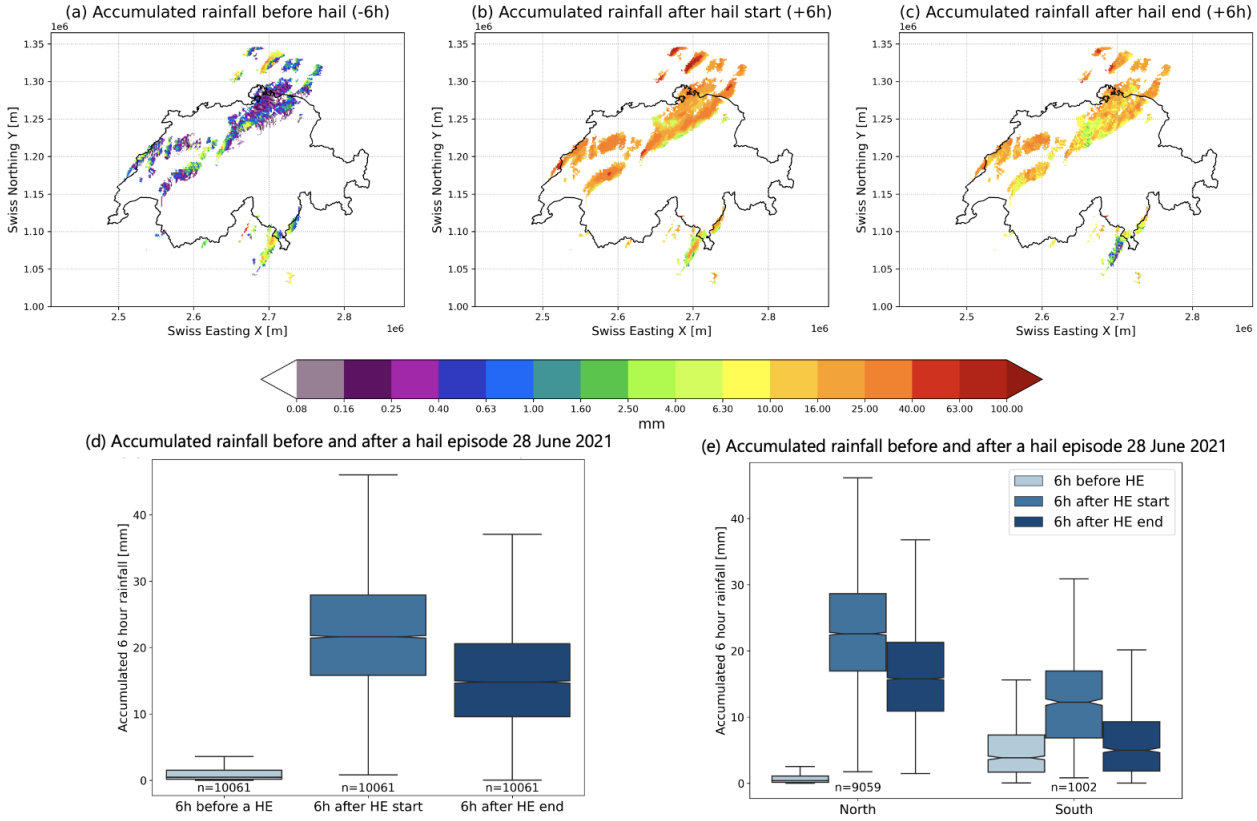

Figure 11: The mean cumulative 6h rainfall on June 28th 2021 (a) before a HE, (b) after the HE initiation, (c) after the end of a HE. (d) summary box plot of all the values from (a-c). (e) same as (d) but separated into northern and southern study areas (outline of the regions in Figure 7). Notched box plots are explained in section 3. n is the number of grid cells affected by a HE.

Figure 11 shows how much rainfall accumulated on 28 June 2021 (a) 6 hours before the HE, (b) 6 hours after the HE start and (c) 6 hours after the end of the HE. (d) quantifies the values of (a-c) in a box plot and (e) further subdivides the results into northern and southern parts (for the regions refer to Figure 7).

Overall, the rainfall is not evenly distributed around a HE. That is, in the whole study area, the cumulative rainfall before a HE is significantly smaller than after the HE (Figure 11 (d)). The median 6-hour cumulative rainfall values are 0.5 mm before a HE, 21.6 mm after the start of a HE and 14.8 mm after the end of a HE. A discussion on the differences of cumulative rainfall amount from the start or the end of a HE are discussed in section 5.2.7.

In the north and south the cumulative rainfall before a HE is significantly smaller than after the start and the end of a HE. In the northern part of the study area, on average per grid cell, only 0.38 mm of rainfall accumulated in the 6 hours before the hail (Figure 11 (a, e)). In contrast, in the 6 hours after the start of the HE, the median value of the accumulated rainfall per 1 km^2 is 22.6 mm and 15.8 mm after the end of the HE. In the northern part, there is a greater accumulated rainfall after a HE, if compared to the south.

In the southern study area, the accumulated rainfall amount on each grid cell is more evenly

distributed before and after hail. The cumulative 6-hour rainfall median values are 3.8 mm before a HE, 12.3 mm after the start of a HE and 5.0 mm after the end of a HE (Figure 11 (e)).

Lastly, an order of magnitude smaller area was affected in the south on the case study day (1002 vs 9059 km^2).

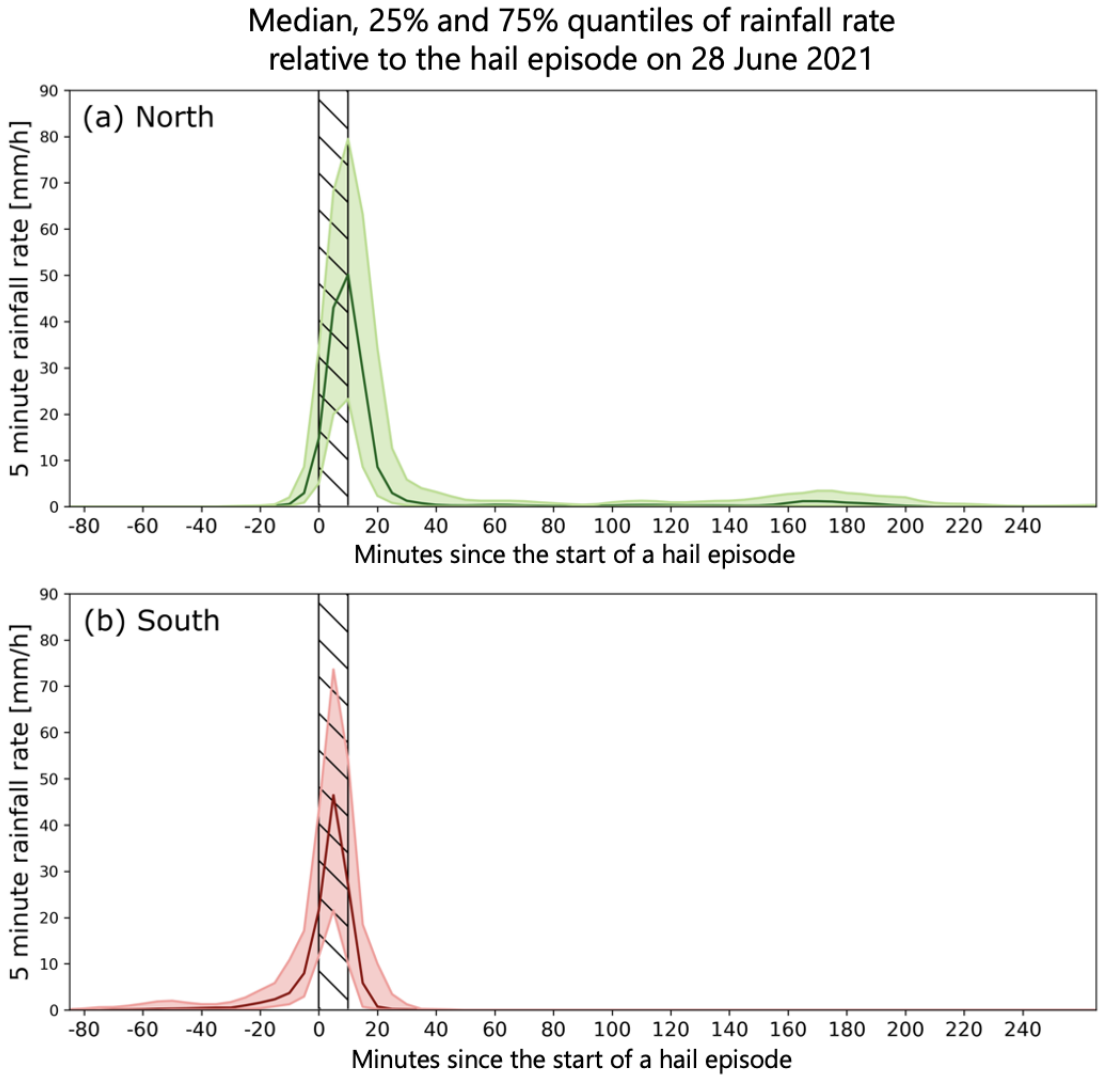

Figure 12: Distribution of rainfall rate on 28 June 2021 in the (a) northern study area, (b) southern study area. Indicates the time evolution of the accumulated 6h rainfall is shown in Figure 8 (e). Dark red and green line is the median, shaded area is between the 25% and 75% quartiles. The hatched area is the average length of a hail episode from the seasonal analysis. The rainfall onset times are determined by when the median rainfall rate is above 0.5 mm/h. The end of rainfall is determined by the time step when the median rainfall rate is below 0.5 mm/h.

Figure 12 shows the median rainfall rate distribution around a hail episode for (a) northern and (b) southern parts of the study area for 28 June 2021. Time from 80 minutes before to 4 hours after a HE is shown. The time span is chosen to display the variability of rainfall rate before and after a HE. The hatched area is the average duration of a HE on the case study day (11 min 35 sec).

There is a difference in the distribution of rainfall rate between the northern and southern parts.

First, in the north, the maximum rainfall rate is observed 10 minutes after the initiation of the HE, compared to 5 minutes in the south. The peak median rainfall rate is 50 mm/h in the north and 47 mm/h in the south and the peak lasts only for 5 to 10 minutes (Figure 12).

The rainfall onset is 15 minutes and 30 minutes before the HE occurrence in the north and south, respectively. The rainfall ends 45 minutes and 25 minutes after the HE start in north and south, respectively.

Next, in both areas, a small "bump" in the median rainfall rate time series is visible as an increase in the median and 75% quantile of rainfall rate. However, in the south, the bump occurs 50 minutes before a HE but in the north 160 minutes after a HE.

4.2 Convective season analysis

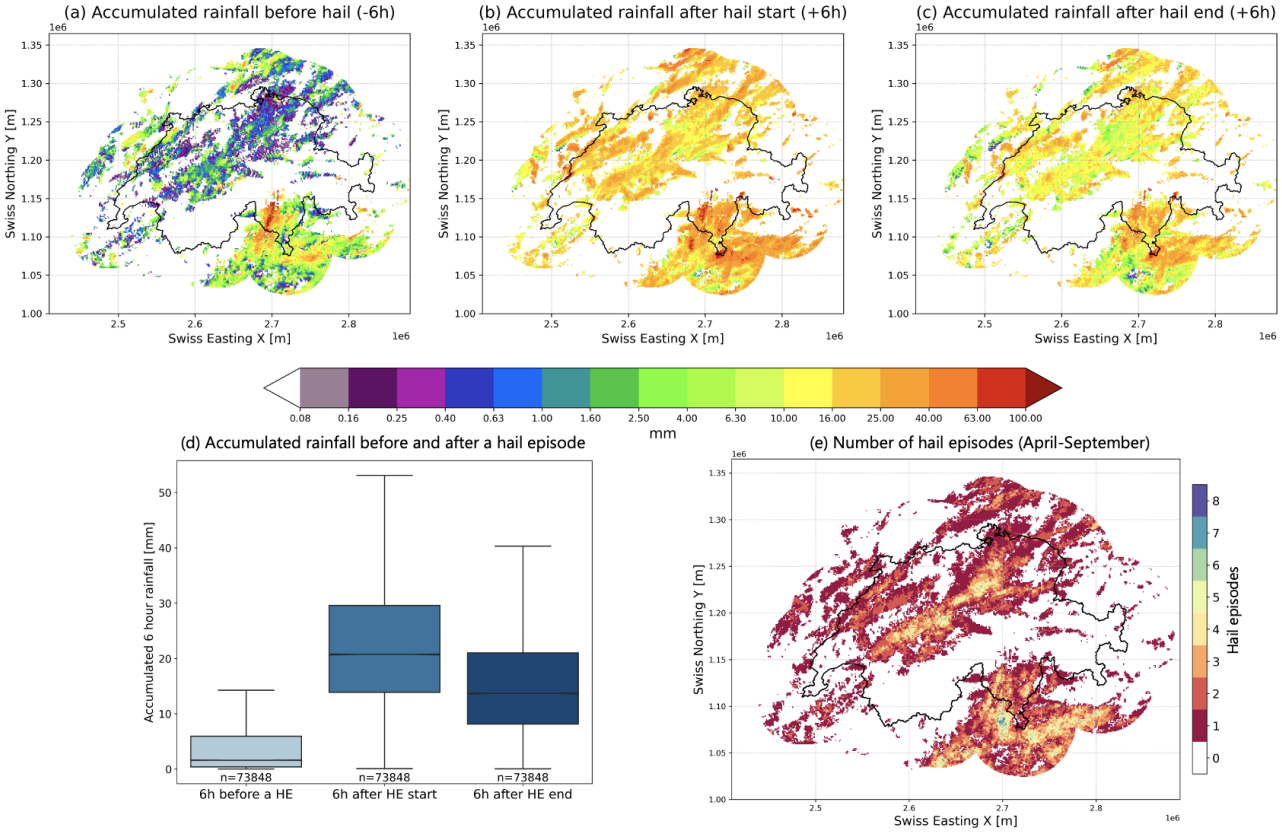

Figure 13: The mean cumulative 6-hour rainfall for the 2021 convective season (a) before a HE, (b) after the HE initiation, (c) after the end of a HE. (d) summary notched box plot of all the values from (a-c). (e) the number of hail episodes in the convective season. n is the number of of grid cells impacted by a HE.

Figure 13 shows the general findings from the cumulative rainfall analysis of the 2021 convective season.

On average, the cumulative rainfall is significantly lower in the 6 hours before a HE, when compared to 6 hours after a HE (Figure 13 (a-d)). That is, the median cumulative rainfall amounts after the start of the HE and after the end of a HE are significantly higher than the rainfall before a HE. The median values are 20.7 mm (6-hour cumulative sum after the start of the HE), 13.7 mm (6-hour cumulative sum after the end of the HE) and 1.6 mm (6-hour cumulative sum before the HE) (Figure 13 (d)). The rainfall before a HE shows lower variability and the distribution is strongly skewed towards 0.

The difference between the cumulative rainfall values before and after a HE is large because even the 25% and 75% quantiles of the box plots do not overlap. Additionally, due to the large data ensemble, notches in the box plots are not visible.

4.2.1 Spatial characteristics

Rainfall association with hail Figure 13 (a-c) shows the mean 6-hour cumulative rainfall before and after a HE for each grid cell for the 2021 convective season. The figure shows that the

cumulative rainfall distribution before and after a HE has a heterogeneous spatial distribution. The area where hail and rainfall co-occur in Figure 13 (a-c) (colored part) is set by the occurrence of hail rather than rainfall. That means, there were no areas that did not experience any rainfall 6 hours before or after a HE.

Figure 13 (e) shows how many HEs during the convective season occurred. The number varies between 0 over the main Alpine ridge, 1-3 over parts of Plateau and Jura (a map with region names can be found in Figure 1). The highest number of HEs occurred in a swath along the Northern Prealps and in the Southern Prealpine region. When comparing the areas where the largest number of HEs occurred (Figure 13 (e)) to the areas with the highest cumulative rainfall amounts (a-c), there is no apparent spatial match.

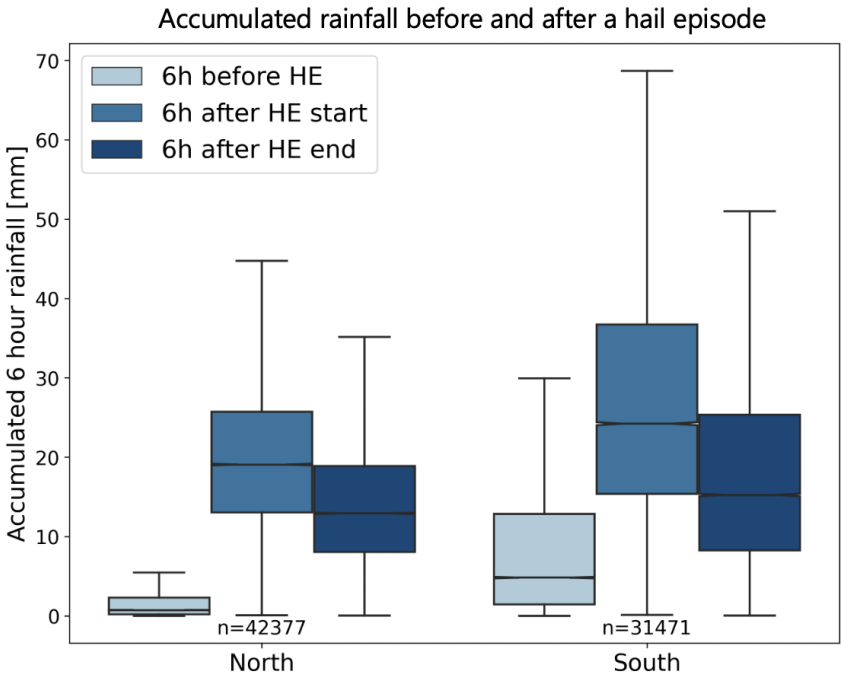

Figure 14: Summary notched box plots of all the values from Figure 13 (a-c) separated into northern and southern study areas (outline of the regions in Figure 7).

North vs south As visible in Figure 13, the difference in rainfall before and after hail is not equal in all regions of Switzerland. This leads us to further explore the spatial differences between the north and south study areas (reference for regions in Figure 7).

Figure 14 shows how the cumulative rainfall before and after a HE differs between the northern and southern study areas. First, there is a significant difference between the cumulative rainfall before and after a HE in both regions. As described previously, both cumulative rainfall sums after the HE are significantly higher than the rainfall before a HE. In the north, the cumulative rainfall median before a HE is 0.7 mm and 19.1 mm after the start and 13.0 mm after the end of a HE. In the south, medians are 4.8 mm before a HE, 24.2 mm after the start of a HE and 15.2 mm after the end of a HE.

Second, southern areas show overall higher median values and a larger spread than north, as

indicated by the height of the boxes and whiskers in Figure 14. Lastly, more HEs are recorded north of the Alps (n=42377), when compared to the south (n=31471). It has to be noted, that the norther study area is larger then in the south.

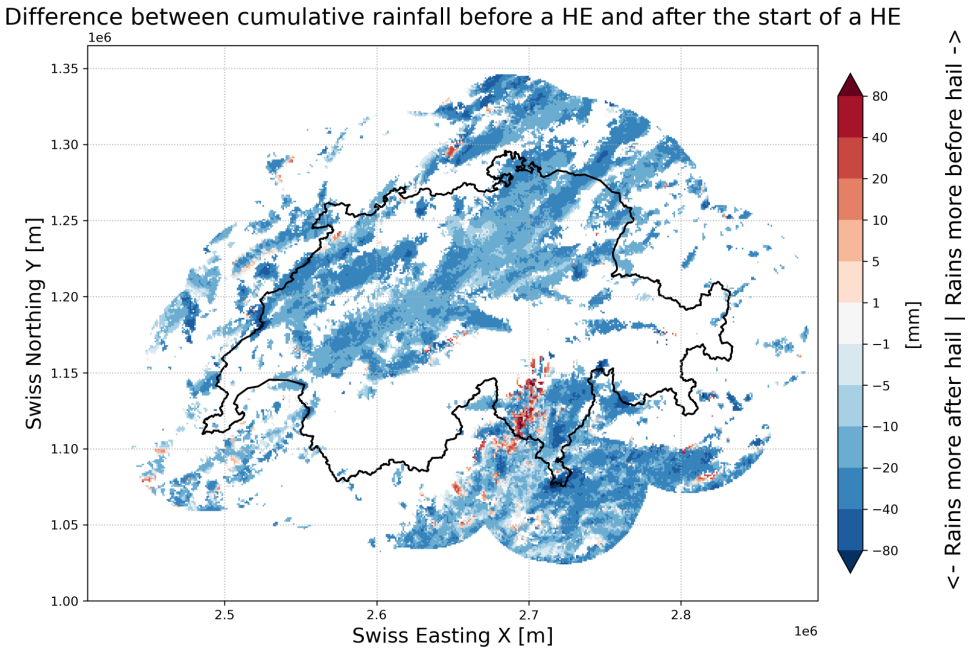

Figure 15: The difference between the average 6h cumulative rainfall before a HE (Figure 13 (a)) and the average 6h cumulative rainfall after the start of a HE (Figure 13 (b)). The red colors indicate more cumulative rainfall before a HE, blue colors more rainfall after the HE.

Figure 15 shows the difference between Figure 13 (a) (the 6-hour cumulative rainfall before a HE) and (b) (the 6-hour cumulative rainfall after the start of a HE). Although both the rainfall before and after a HE is spatially varied, the difference shows that in a small, elongated area around the Lago Maggiore in Ticino, rainfall is higher in the 6 hours before a HE. Also Figure 13 (a) shows that there is a defined ellipsoid area in Ticino where the rainfall before a HE is higher (around 40-60 mm) compared to the surrounding areas (2.5-25 mm).

4.2.2 Time evolution of rainfall around a HE

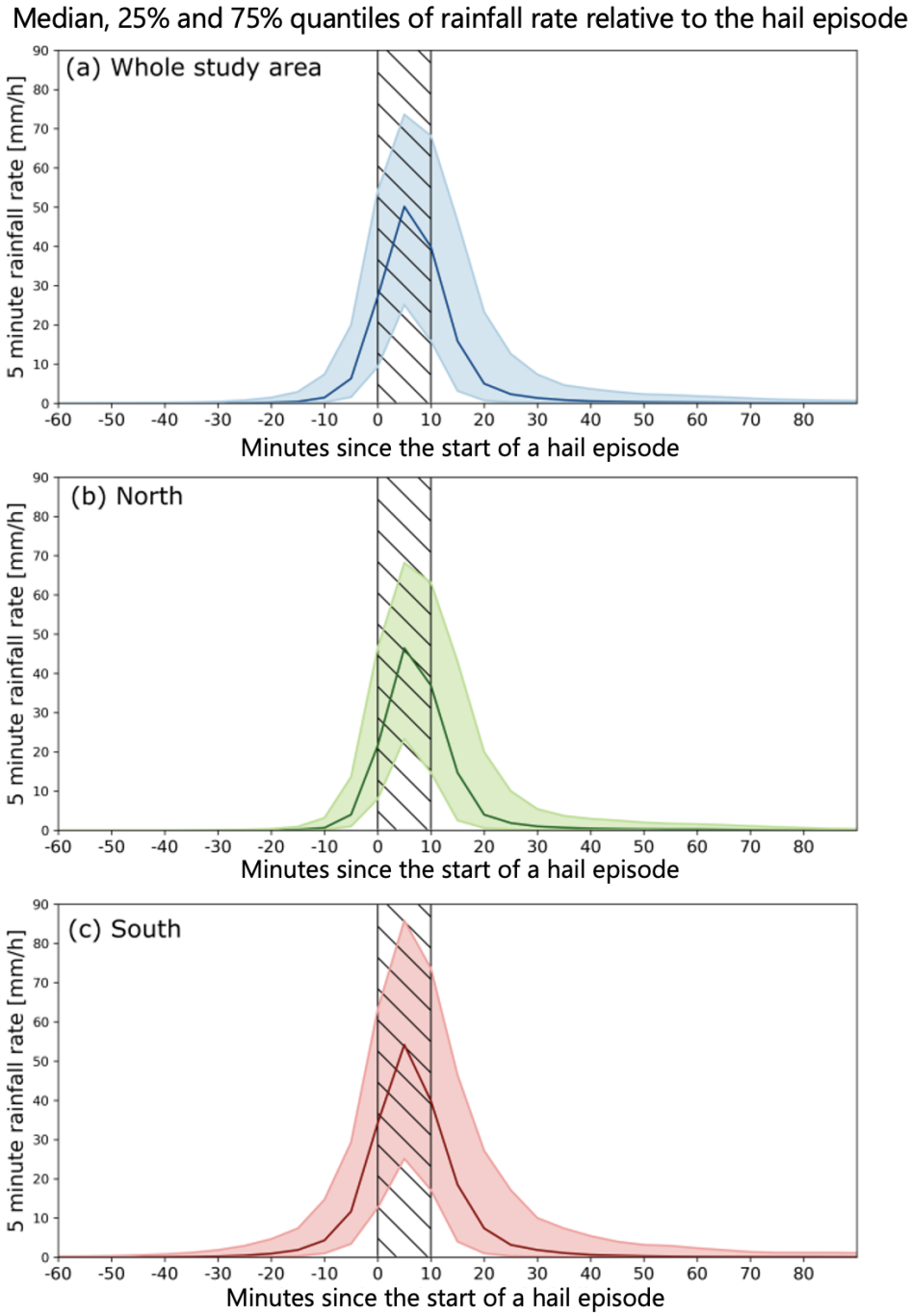

Figure 16: Distribution of rainfall rate in the (a) whole study area, (b) northern study area, (c) southern study area. Indicates the time evolution of the accumulated 6h rainfall is shown in Figure 13. The dark lines are the median values at every time step, shaded area is between the 25% and 75% quartiles. The hatched area is the average length of a HE per grid cell. The rainfall onset times are determined by when the median rainfall rate is above 0.5 mm/h. The end of rainfall is determined by the time step when the median rainfall rate is below 0.5 mm/h.

To determine when the main contributions to the cumulative rainfall occur, the time evolution of rainfall rate is explored. Figure 16 shows how the average rainfall rate is distributed around a HE. Considering the entire 2021 convective season, the mean duration of a HE per grid cell is 10

minutes 20 seconds, which is represented as the hatched region in the line graphs. Only -60 to +80 minutes around the HE are shown because the values further in either direction are close to 0.

The seasonal-median distribution of rainfall around a HE is similar across the whole study area, showing that most of the accumulated rainfall occurs very close in time to the HE (Figure 16). In all considered areas the rainfall rate peaks 5 minutes after the start of the HE. Peak rainfall rates are 45 mm/h in the north and 56 mm/h in the south.

There is a difference in rainfall onset and end times between the north and the south (Figure 16 (b, c)). The average rainfall onset is 15 minutes and 25 minutes before a HE in the north and south respectively. The end of the rainfall is 40 minutes and 45 minutes after the HE start in the north and south respectively. This means that in the south on average there is a longer time window in which rainfall occurs around a HE, when compared to the north.

In Figure 16 no additional "bumps" in the rainfall rate before or after the main rainfall peak are observed. Such "bumps" are visible in, for example, Figure 12 and 19.

4.2.3 Monthly and diurnal variability

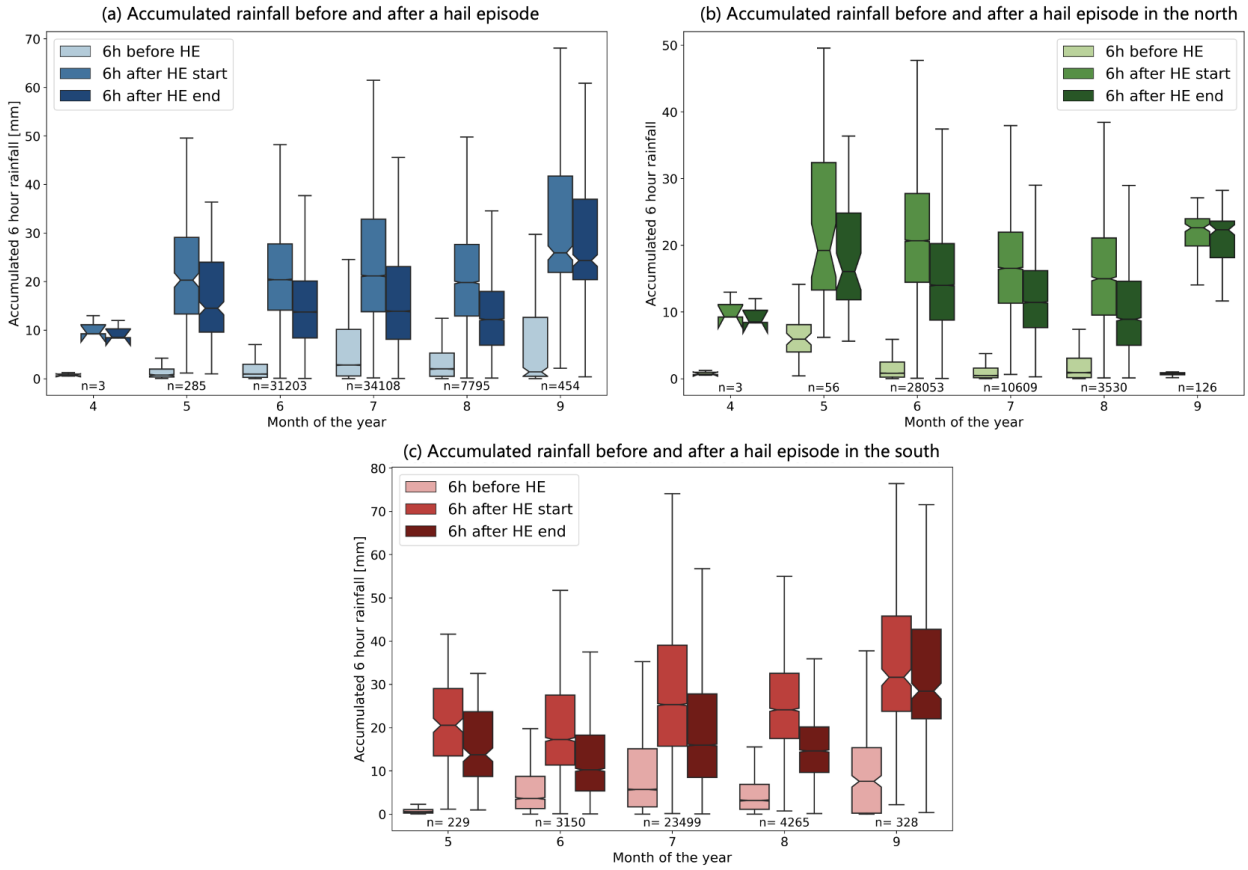

Figure 17: 6h cumulative rainfall around a HE separated by the month of the HE occurrence. (a) whole study area, (b) northern, (b) southern study areas. Notched box plots are explained in section 3. Data only from the 2021 convective season is presented.

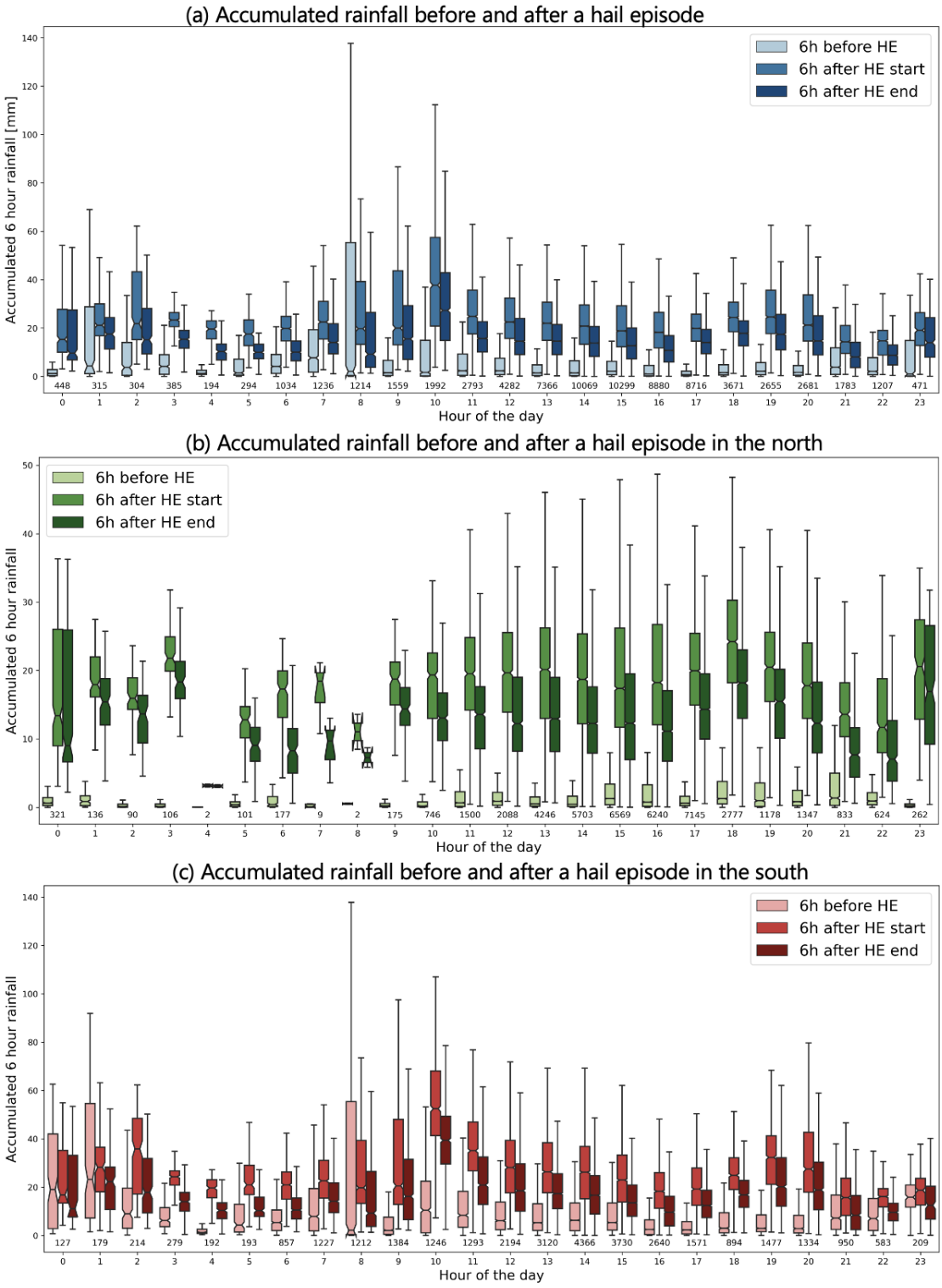

Figure 18: Same as Figure 17 but separated by the hour of the HE occurrence (UTC). Note the different y-axis lengths. Data only from the 2021 convective season is presented.

In this section, monthly and diurnal differences of rainfall before and after a HE are analysed for different sub-regions for the 2021 convective season.

Monthly variability Figure 17 shows how the cumulative rainfall before and after a HE changes between months of the 2021 convective season. In all months except April, the cumulative rainfall before a HE is significantly smaller than the cumulative rainfall after the start and end of the HE. This is expected, as there are only 3 data points in the month of April.

In the spring and autumn months, there are fewer HEs (3-450) than in the summer months (7,000-34,000) with June and July showing the highest values.

The median cumulative rainfall around a HE is different for each of the months and the investigated areas. The summer months do not show the highest median values of accumulated rainfall. In Figure 17 (c) it is visible that, especially in the south, the rainfall values in September are higher before and after hail when compared to the other months. Median values in September are 7.5 mm before the HE, 31.6 mm after the start of a HE and 28.4 mm after the end.

Diurnal variability If the whole study area is tested together, regardless of the time when a HE was initiated, the cumulative rainfall before a HE is significantly smaller than after a HE (Figure 18 (a)). Here intra-hourly variability refers to the height of the boxes (range between 25% and 75% quantiles) and inter-hourly variability refers to the comparison of medians and boxes between hours.

In the north, the rainfall after a HE is almost always significantly higher than rainfall before the HE. The exception is when a HE occurs at 0400 or 0800 UTC, when the difference between the cumulative rainfall before and after a HE is not significantly different. It is attributed to having only 2 data points in each hourly group.

Figure 18 (b) shows that in the north the cumulative rainfall after a HE has a larger intra-hourly and inter-hourly variability, than the rainfall before a HE. The median cumulative rainfall value before a HE is similar regardless of the hour when the HE occurs (medians range from 0.1 mm at 0200 UTC to 1.3 mm at 2100 UTC). The intra-hour variability of the rainfall before a HE increases in the second part of the day (1100-2200) (Figure 18 (b)). The cumulative rainfall after a HE peaks at 1800 (median is 24.2 mm after the start of a HE and 18.2 mm after the end of a HE). The large inter-hourly variations of the rainfall after a HE between 0100 and 0800 are likely related to a very small data pool for each of the hours. In the south, there is higher intra-hourly and inter-hourly variability in the rainfall before a HE when compared to the north (Figure 18 (c), note the different y-axis).

The cumulative rainfall after a HE in the south peaks at 1000 UTC (median 52.4 mm after the start of a HE, 39.3 mm after the end of a HE), with two smaller peaks at 1900 (median 32.3 mm after the start, 20.2 mm after the end of a HE) and 0200 UTC(median 22.3 mm after the start, 22.2 mm after the end of a HE).

In the south, at 0000 and 0100 UTC the cumulative rainfall after the start of a HE is not significantly higher than the rainfall before a HE. Moreover, if the rainfall after the end of a HE is considered, then also at 2100 and 2200 UTC the median rainfall value before the HE is not significantly different from the rainfall after the HE (Figure 18 (c)).

Next, because of the intriguing results in Figure 18, I want to explore whether the rainfall during the night hours has the same distribution around a HE, as the whole southern region on average (Figure 16 (c)). Figure 19 shows the evolution of rainfall rate for HEs that occur from 2100

to 0100 UTC in the southern parts of Switzerland. It is visible that -110 and -50 minutes before the HE there is a small increase in the 75% quantile in the rainfall rate.

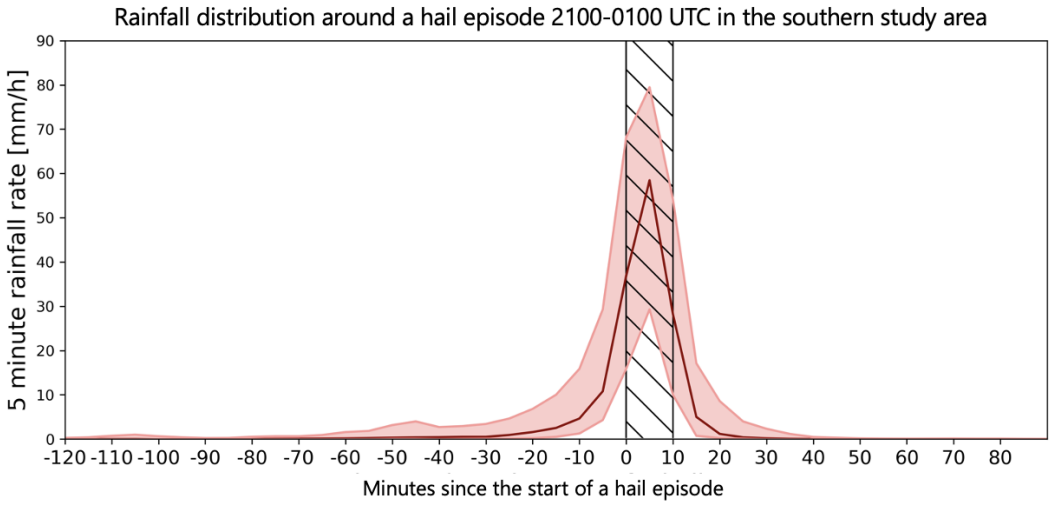

Figure 19: Same as Figure 16 (c) but only for the hours 2100-0100 UTC in the southern part of the study area.

4.2.4 The effect of estimated hail size

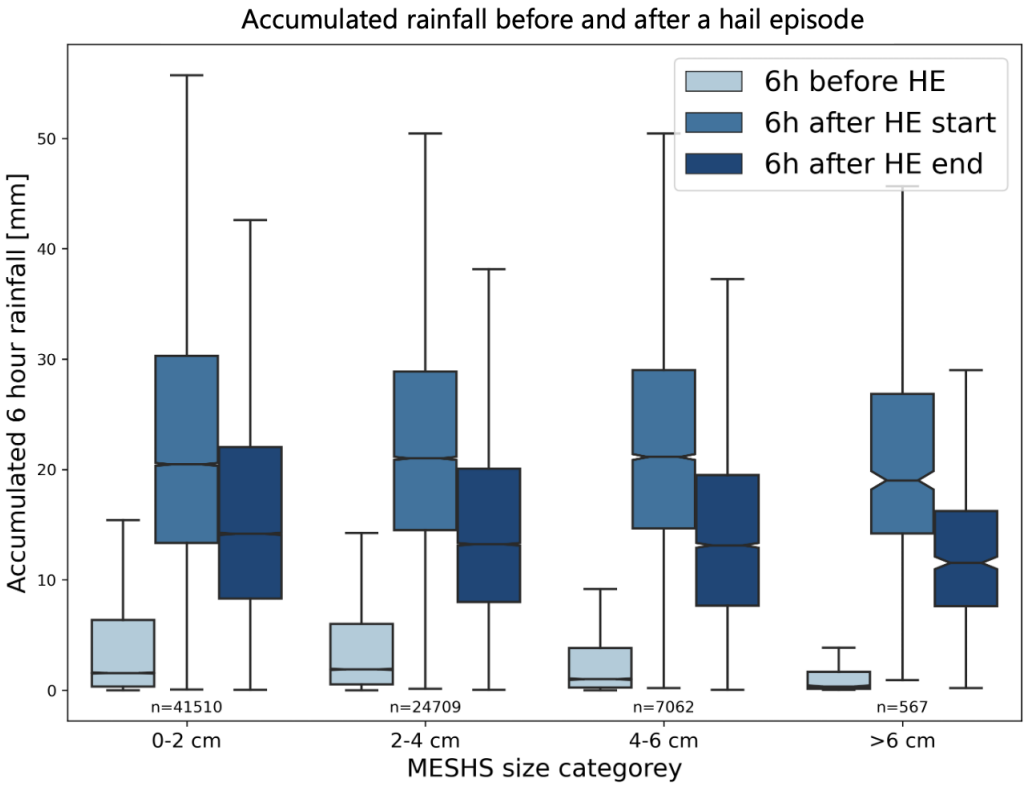

Figure 20: Same as 14 but separated by the recorded MESHS size at the time step when the HE was initiated.

Figure 20 shows the cumulative rainfall before and after a HE for different hail size groups. Firstly, more than 55% of HEs are associated with small hail stones (0-2 cm diameter). The number of observations steeply decreases with increasing MESHS group size.

In all hail size groups the cumulative rainfall before a HE is significantly smaller than after a HE. The maximum estimated hail size does have a small relation to the rainfall amount before and after a HE when compared between hail size groups. There is a decrease in median rainfall values before a HE with increasing hail stone size. The medians decrease from 1.6 mm (0-2 cm hail size) to 0.3 mm (>6 cm hail size).

For the sake of brevity, only the cumulative rainfall after the start of the HE is reported and discussed in the current and the following results sections (4.2.5, 4.2.6). The cumulative rainfall after the start of a HE is the lowest for the largest hail size class (19 mm) and highest for the 4-6 cm size class (21.1 mm).

4.2.5 The effect of fronts

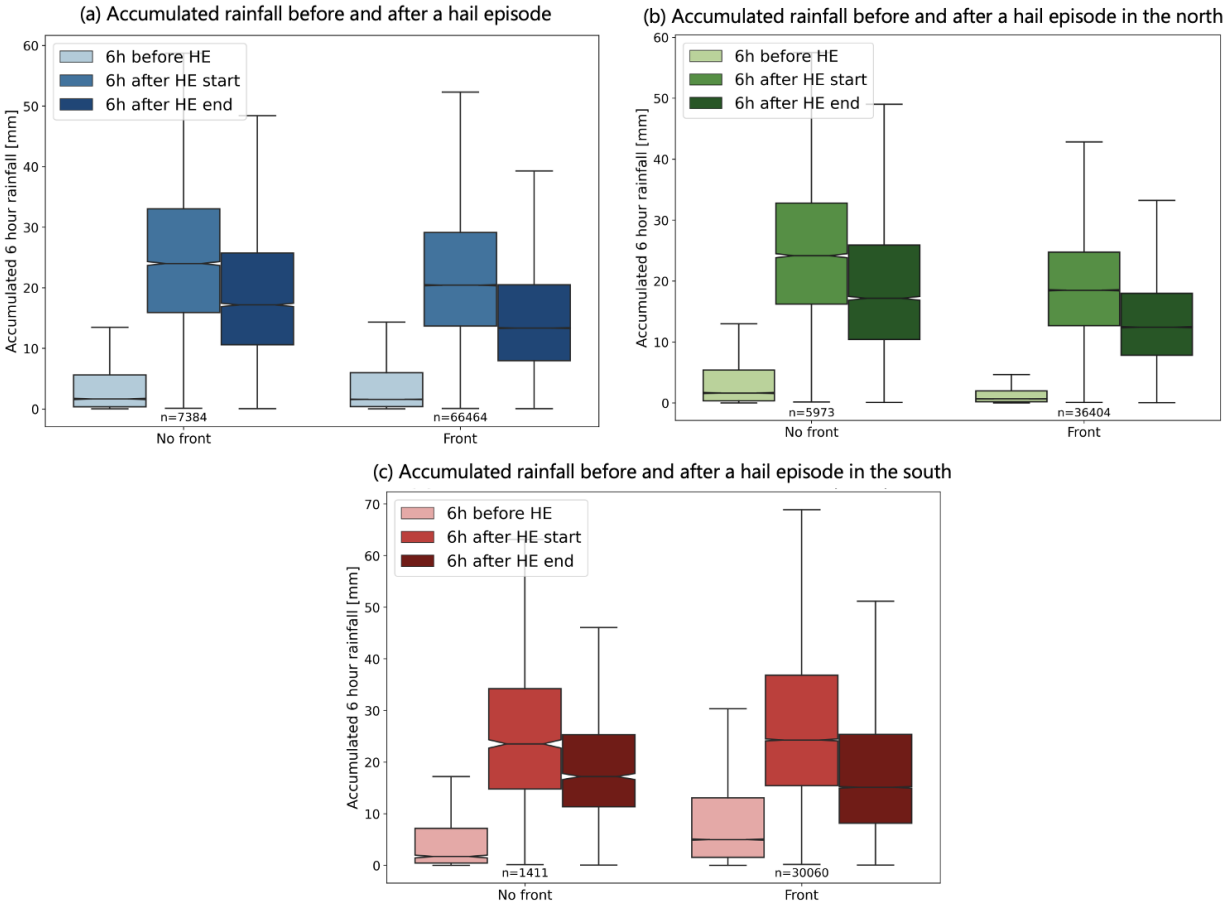

Figure 21: Same as Figure 17 but the hail episodes are separated into groups depending on the frontal situation on the day of hail occurrence. (a) for all study area, (b) for northern and (c) for southern parts of the study area.

Figure 21 shows how the accumulated rainfall varies depending on the presence of a front.

First, almost an order of magnitude fewer HE are recorded when no fronts are present compared to the group with a front present (7384 HE with no front vs 66464 HE associated with a front).

In all considered cases, the cumulative rainfall before a HE is significantly smaller than the cumulative rainfall after the HE. Next, if the whole study area (Figure 21 (a)) is considered, then the presence of a front does not seem to impact the rainfall before a HE (both medians 1.6 mm). In the whole study area together, the presence of a front leads to a lower accumulated median rainfall after the HE. The medians are 24.0 mm when no front is present and 20.4 mm when a front is present.

In Figure 21 (b, c) the effect of fronts on the cumulative rainfall in northern and southern parts of Switzerland is shown. In the north, the presence of a front leads to a lower median and lower variability of rainfall before and after a HE, as indicated by the height of the box plot and whiskers. The median cumulative rainfall value before a HE is 1.6 mm when no front is present and 0.6 mm when a front is present. The median cumulative rainfall value after a HE is 24.1 mm when no front is present and 18.1 mm when a front is present.

In the southern area, the results are not consistent with the observed values in the north. In the south, the presence of a front leads to a higher cumulative rainfall before a HE than without a front. The median cumulative rainfall value before a HE is 1.7 mm when no front is present and 5.0 mm when a front is present. The median cumulative rainfall value after a HE is 23.5 mm when no front is present and 24.1 mm when a front is present.

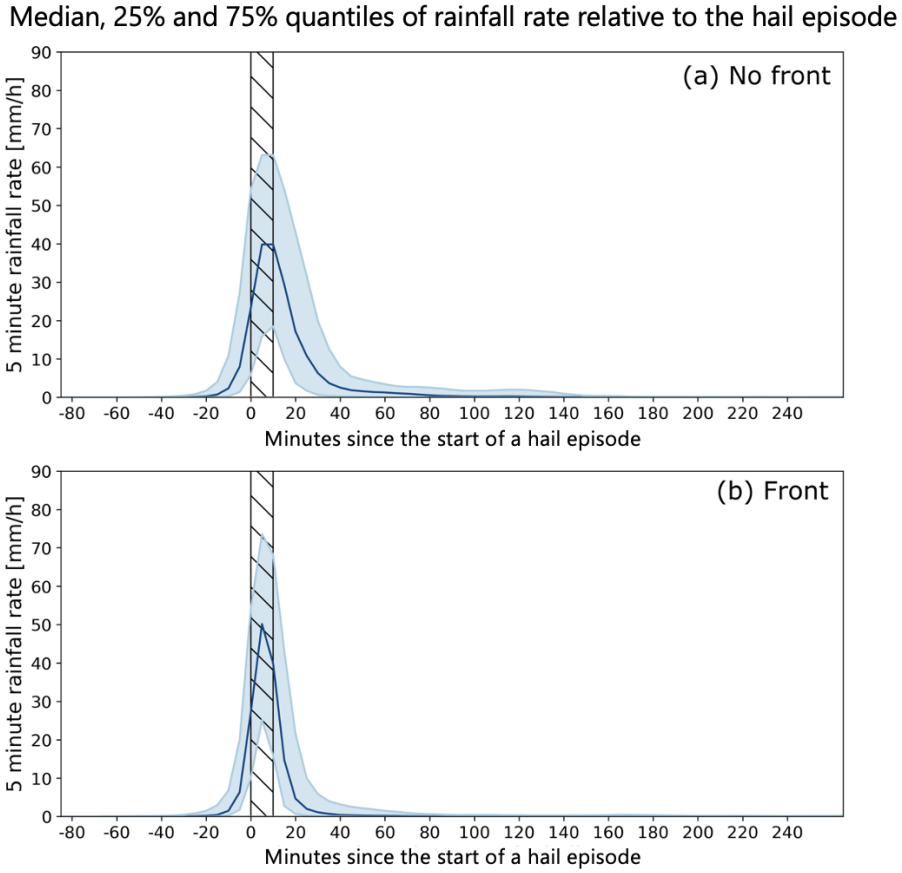

Figure 22: Same as Figure 5.2.2 but HEs subdivided into groups where (a) no front was present, (b) a front was present on the day when the episode occurred.

Figure 22 shows how the rainfall rate is distributed around a HE for the cases that (a) are not associated with a front or (b) that occur when a front is present. It is visible that, when no front is present, the peak in the rainfall rate is lower (42 mm/h median and 67 mm/h 75% quantile), when compared to the cases with a front (50 mm/h median and 72 mm/h 75% quantile).

In the case when HE occurs without a front present, the rainfall in a grid cell lasts longer after a HE than in the presence of a front. The onset time of the rainfall is the same in both front groups (20 minutes before the start of a HE). The end of the rainfall in a grid cell on average is later in the cases without a front. The end of the rainfall is 85 minutes after the HE start in the cases with no fronts and 45 minutes after the HE start in the cases with fronts.

4.2.6 Sensitivity analysis

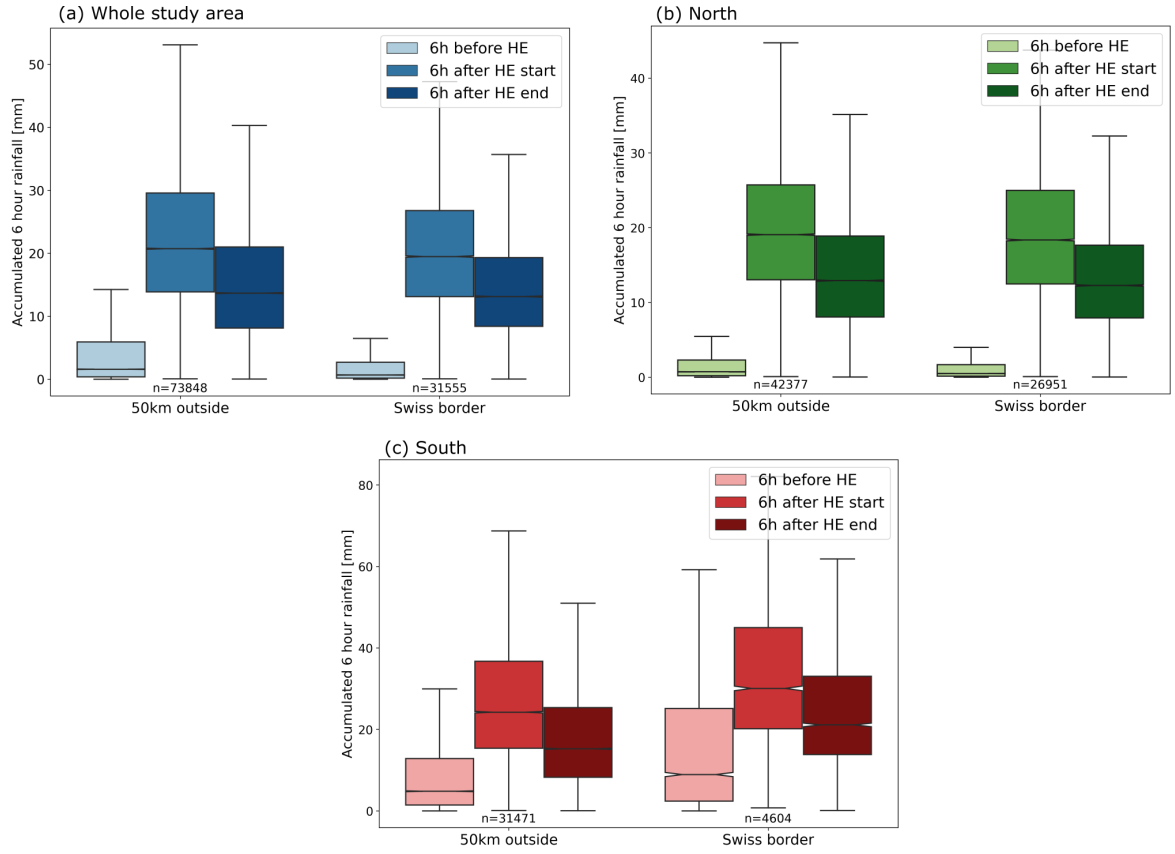

Figure 23: Same as Figure 17 but separated by whether the HE occurred within Swiss territory or in the whole study area. Note the different y-axis lengths.

Swiss territory vs the study area Figure 23 shows the rainfall before and after a HE for the grid cells within Swiss borders and across the whole study area. The reason behind exploring the differences in the median cumulative rainfall amounts between these two areas are described in Section 5.2.7.

First, in all cases and areas considered, the median cumulative rainfall before a HE is signifi-

cantly smaller than after the HE. In the north (Figure 23 (b)), there is a small difference between the median cumulative rainfall values within the Swiss territory and in the whole study area. The median value within the Swiss borders before a HE is 0.5 mm and the median value after the start of a HE is 18.3 mm. Over the whole study area, the median before a HE is 0.7 mm and the median value after the start of a HE is 19.1 mm.

In the south (c), interestingly, the values within the whole study area are smaller than only within the Swiss borders. The median values in the Swiss territory are 8.9 mm before a HE and 30.1 mm after the start of a HE. The median values in the study area are 4.8 mm before a HE and 24.2 mm after the start of a HE.

5 Discussion

This section of the thesis discusses the results of the case study (5.1) and the convective season analysis (5.2) and compares the results to the current literature.

5.1 Case Study 28th June 2021

5.1.1 Hail and rain events

Overall, the large area that HEs and REs covered on 28 June (Figure 8) suggests that there was widespread convective activity. Kopp et al. (2022) indeed reported that storms had the second-largest recorded area of severe (at least 100 km^2 of MESHS $\geq$ 4cm) and extreme (at least 100 km^2 of MESHS $\geq$ 6cm) hail north of the Alps in Switzerland. Hail and heavy rainfall are observed on the northern and southern Prealps, Plateau and the Jura region, while the main alpine chain is not affected, which is in agreement with the climatology in Switzerland (Panziera et al., 2018; Nisi et al., 2016; NCCS, 2021).

Figure 8 shows that in the most heavily affected areas reported (northern Switzerland), only one RE occurred. Most of the multiple RE occurrences are south of the Alps. The high number of REs in the south can be attributed to the definition of RE. The definition is linked to an extreme rainfall threshold in northern Switzerland. However, in the south, the same threshold is no longer extreme, as the south is characterised by more intense rainfall (Barton et al., 2020). For more information on thresholds see Section 3.

The high number of REs in a linear streak close to Lago Maggiore which are visible in Figure 8 (a) are similar to the echo training events explored in Panziera et al. (2015). A more detailed discussion on this phenomenon is in Section 5.2.1.

Co-occurrence area Now the similarities and differences of the spatial distribution of HEs and REs are discussed.

Light rainfall rate was registered over all of the areas where a HE occurred. Extreme rainfall occurred in 85% of the grid cells that experienced a HE (Figure 8 (c)). Therefore, most of the HE-affected area was also affected by a RE.

In Figure 8 (c) it is shown that most of the areas that experienced hail but not extreme rainfall are on the edges of the co-occurrence area. It can either be attributed to the hail storm dynamics or it is a radar measurement error signal. In the current analysis, it is not possible to explain this pattern, because a model of the storms on the case study day is likely necessary to explore the small scale dynamics that might lead to these results.

Figure 8 (a, b) shows a good spatial match of HE and RE in the northern part. On the contrary, in the south, the area of the largest HST is not co-located with the area of the highest rainfall (streak with multiple REs). The fact that extreme rainfall and hail areas are not overlapping likely contributes to the smaller damages observed in the south.

The majority of the hail-affected area is subjected to a likely hail-rainfall compound event due to the overlap of the areas of RE and HE occurrence. To say whether there was a compound event, the occurrence times have to be compared, which is done in the next subsection (5.1.2).

In summary, the areas affected by HEs and REs on June 28^{the} 2021 agree well with the hail and rainfall climatologies. 85% of the area that was affected by hail is also affected by extreme rainfall.

5.1.2 Co-occurrence sequence

The answer to the question "In what sequence did the hail and rainfall occur in the co-occurrence area?" depends on the chosen rainfall threshold. Figure 10 (a) shows that most areas where hail and rain co-occurred first experienced at least light drizzle before the HE. This result agrees with previous studies, as a convective storm is usually first detected without a hail footprint (Nisi et al. (2018)).

Extreme rainfall in almost 90% of the co-occurrence area occurs within the same 10-minute period as the HE. This suggests that the majority of the area experienced hail and extreme rainfall compound event in a sequence that can lead to the largest damages, that is, HE and RE in close temporal proximity, thereby creating a compound event.

In the north, a short time lag between HE and RE occurrence per grid cell and the good spatial match in RE and HE occurrence suggests that in each grid cell, rainfall and hail episodes came from the same convective system. The same conclusions cannot be made about the south due to multiple RE occurrences.

In Figure 10 and 9 "fishbone pattern" in the radar reflectivity measurements is visible. This might indicate likely error or uncertainty in the comparisons of the occurrence time steps. The problem is further explored in Section 5.3.

In summary, the time difference between hail and rainfall occurrence is not uniform everywhere but, in general, some amount of rainfall is recorded in all areas before hail is registered. Hail and extreme rainfall on 28 June 2021 occurred close in time (+/- 10 minutes) from each other. That is, there were large areas over Switzerland where a hail-rainfall compound event was created, which led to the great reported damages.

5.1.3 Cumulative rainfall before and after hail

Lastly, the 6-hour cumulative rainfall before and after a HE was explored for the case study day. Figure 11 shows the main results that there was significantly lower cumulative rainfall before a HE, when compared to the cumulative sum of rainfall after the HE.

The results show a higher rainfall accumulation per 1 km^2 after the HE in the north when compared to the south. This is an unusual result because on average, the rainfall intensity is higher south of the Alps (Feldmann et al., 2023; Panziera et al., 2018). Interestingly, Figure 12 shows that the peak rainfall rate was similar in both northern and southern study areas. Therefore, the higher cumulative rainfall after the HE in the north is likely explained by the on average longer-lasting rainfall after the HE (Figure 12). The longer post-HE rainfall in the north can be attributed to the occurrence of a mesoscale convective system (Kopp et al., 2022), which is associated with large areas of heavy stratiform rainfall (Houze Jr, 2004). The other possible contribution to the high cumulative rainfall after the HE in the north is additional rain storms that followed after the HE. This idea is further explored below.

In both regions, the maximum rainfall contributions to the accumulations occur very close in time to the HE (Figure 12). This is in agreement with Figures 10 and 9, which indicated extreme rainfall in the same 10-minute interval as hail. From previous figures, however, it was not clear if the extreme rainfall close to hail was the only major contributor to the cumulative rainfall after the HE. Figure 12 further adds to the results by showing that on the case study day, it is the extreme rainfall around the HE that forms the majority of the rainfall accumulation for any area.

In Figure 12 small "bumps" are visible outside the main rainfall rate peak which occurs around the HE. The "bumps" can be interpreted as additional rain storms crossing the area before or after the HE. However, by using only the current data, it is hard to precisely determine whether the small "bumps" show the rainfall from the same system that created a HE, or a different one. The possible solutions to explore this with different data sets are discussed in section 6.3. However, given the long time difference between the main rainfall rate peak and the small "bumps" in rainfall rate (more than 2 hours), it is suggested that in the north additional rain storms contributed to the cumulative rainfall after the HE.

Compared to the main rainfall peak, the contribution from likely separate rain storms on the case study day is on average small. It is likely that locally this contribution can be larger but due to averaging over many HEs, the signal is lowered.

Hohl et al. (2002) described how the contributions to the damages of multiple convective cells are not proportionally additive. The loss increases dramatically with each consecutive cell crossing the same area. Therefore, although the contributions to the cumulative rainfall of an additional rain storm in the north (140 to 200 minutes after the HE) might not be large, their effect on the damages was likely large. The same cannot be applied to the additional rain storms that precede hail in the south, as there were no hail damages at the time to exacerbate.

In summary, this case study shows that on 28 June 2021, there was high convective activity with one hail episode per grid cell over the study area. In the northern part there was also only one rain episode, but in the south some areas experienced up to 5 rainfall episodes. 85% of the area where hail occurred also experienced extreme rainfall. The time difference between the HE and RE is small and in 88% of the area hail and extreme rainfall occurred in the same 10-minute time interval. Cumulative rainfall before and after the HE is spatially varied. However, overall the 6-hour cumulative rainfall before a HE is significantly smaller than the rainfall in the 6 hours after the start of the HE. There was a higher amount of accumulated rainfall for 1 km^2 after a HE in northern Switzerland, when compared to the southern areas. It is likely that additional rain storms contributed to the high cumulative rainfall after the HE in the north.

There is no previous literature that could be used to compare the current results of the rainfall amounts before and after a HE. Therefore, the results are only compared to the convective season analysis conducted in this thesis. The comparison is in subsection 5.2.6.

5.2 Convective season analysis

Overall, the 6-hour cumulative rainfall amount before a HE is significantly lower than the 6-hour cumulative rainfall amount after a HE (Figure 13). These differences in the cumulative rainfall can be likely explained by the precipitation interaction with the updraft. That is, rainfall and hail are produced in the same updraft and at the same time. However, because the hail stones are larger and heavier, the updraft is not able to keep them suspended afloat at an earlier time than the lighter raindrops (assuming constant updraft speed). Moreover, if falling from the same height, hail reaches the ground earlier because of a higher terminal velocity. Finally, when the environmental conditions are no longer suitable for hail production, like a weaker or smaller updraft, rain drops are still able to form and precipitate in these conditions, therefore leading to a longer time span of rainfall after hail. All of these factors likely allow hail to occur on the ground earlier than heavy rainfall.

It is not surprising that the occurrence of hail is associated with a large amount of cumulative rainfall, because Feldmann et al. (2023) found that 2/3 of all hail and severe hail storms are also rain and severe rain storms.

5.2.1 Spatial characteristics

Comparison to hail and rainfall climatolgoies Although the general spatial pattern of hail frequency distribution in Figure 13 (e) is similar to the climatology of Nisi et al. (2016) and MeteoSwiss (2023) (Figure 3), the distinct peak of hail frequency in the southern tip of Ticino is shifted to the west. It illustrates the high interannual variability of hail occurrence (Nisi et al., 2018). Additionally, The results in Figure 13 show spatial agreement with previous studies that show very little convective activity over the main Alpine chain (Nisi et al., 2016).

Another conclusion that can be drawn from Figure 13 (a-c, e) is that is the number of HEs that an area experiences is not directly linked to the rainfall before or after the HE.

Southern areas show overall higher median values of the cumulative rainfall and a larger spread of the values than in the north. It is in agreement with previous rainfall studies in Switzerland that show overall more rainfall in the south (Feldmann et al., 2023; Panziera et al., 2018). This can be attributed to the warm and moist Mediterranean environment, where convection is favoured over the environment in northern Switzerland (Feldmann et al., 2023). The larger cumulative rainfall variability in the south can likely be attributed to the fact that southern Switzerland shows a weaker diurnal cycle in hail and rainfall occurrence (Figure 4) (Nisi et al., 2016; Barton et al., 2020). It is possible that due to the weaker diurnal cycle in the south, additional storms more often contribute to the cumulative rainfall before and after hail. In the north, hail and rainfall diurnal cycles are more pronounced and the peak times of hail and rainfall coincide (Nisi et al., 2016; Barton et al., 2020), therefore it is less likely that a rain storm will precede or follow a hail storm. Moreover, Feldmann et al. (2023) found that the more severe the storm, the faster its transitional speed. This means that rain storms tend to move slower than hail storms. Therefore, if more additional storms contribute to the rainfall before or after the HE, their contribution can be increased because the accumulation time is longer than for the hail storm.

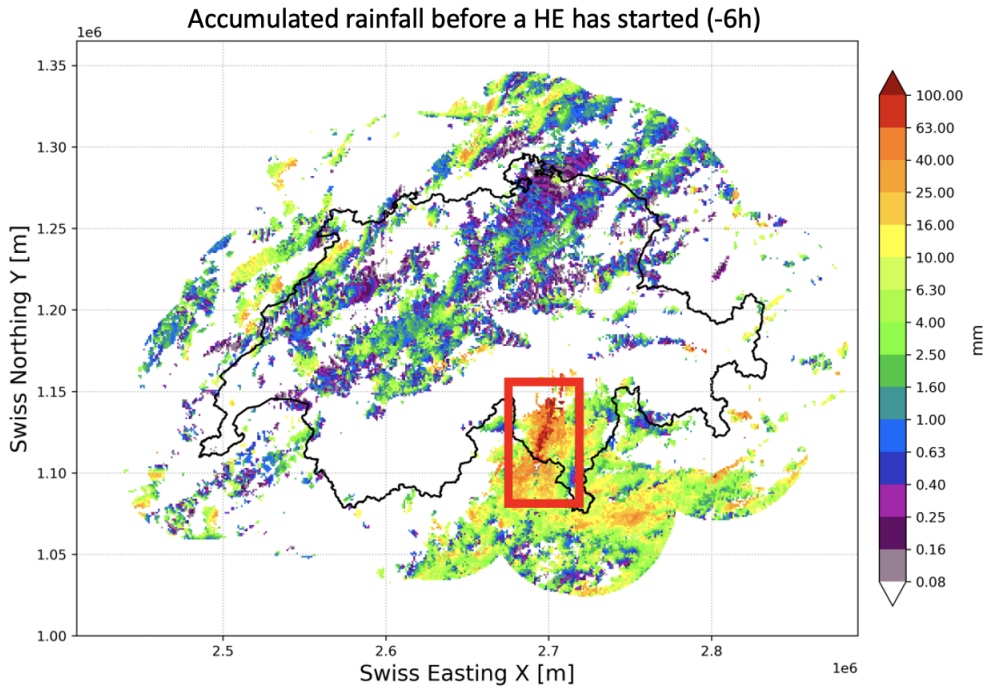

Figure 24: The mean cumulative 6-hour rainfall before a HE for the 2021 convective season. The red box indicates the area of the streak.

Streak in Ticino Figure 13 (a) and Figure 15 show that there is a defined ellipsoid area in Ticino, where the rainfall before a HE is higher compared to the surrounding areas. This streak likely comes about because of echo training, when convective cells move over the same area repeatedly (Schumacher and Johnson, 2005; Panziera et al., 2015). Panziera et al. (2015) observed a similar ellipsoid streak when they looked at flash floods in the southern Alpine region. They proposed a model that can describe how the orography, low-level and upper-level flows interact to facilitate repetitive generation and similar storm tracks in this region (described in more detail in Section 1.2.2). It is likely that this mechanism is at play here. Panziera et al. (2015) looked at the vertical structure of these storm trains. They found that the cells in general were shallow (4-5 km) and the highest reflectivity was recorded below the freezing level. They concluded that heavy rainfall is created by raindrop coalescence. The results from this thesis additionally show that one or more of these consecutive convective cells can be strong and deep enough to develop hail, rather than just rainfall. In addition, Figure 13 (a-c) shows that the convective cells that produce hail are not the first ones of the echo train, as there is a high amount of rainfall before the HE.

Figure 15 also suggests that the more equal cumulative rainfall before and after a HE in the south (Figure 14) likely comes about due to this streak, instead of the general rainfall patterns in the whole southern region. This is because the streak is the only area where the cumulative rainfall values before a HE are higher than the rainfall values after the HE.

5.2.2 Time evolution of rainfall around a HE

By looking at the rainfall rate distribution around a HE in time, it is possible to investigate when the main contributions to the cumulative rainfall before and after a HE occur. Given that the

previous results showed differences in cumulative rainfall around a HE between north and south, in Figure 16 the rainfall rate distributions are shown for each area separately.

The average length of a HE per grid cell (10 min 20 sec) can be compared to the Nisi et al. (2018) Lagrangian hail streak duration. The HE duration per 1 km^2 is smaller compared to the HST duration following a hail storm (25-65 min). This result might indicate that, on average, hail storms do not tend to be stationary, as the time spent over one grid cell is considerably smaller than the average duration of a hail streak in the storm. When comparing the results from this thesis to a climatology, one has to be aware that there is interannual variability that can impact the results of just one season. However, Aregger (2021) found that stationary storms occur only in 3-4 % of the cases, therefore it is more likely that the hail storms tend to propagate and therefore lead to shorter HE duration per 1 km^2.

The time series of rainfall rate around a HE in Figure 16 show a strong rainfall rate peak at the time of the HE. Due to the possible errors associated with rainfall estimates at the time of hail, it is likely that this peak arises from the increased reflectivity due to hail occurrence, rather than just high rainfall rates. However, heavy rainfall during hail episodes is reported (Goodman et al., 1988), so the results are likely not only due to biases in the CPC data. Indeed, Feldmann et al. (2023) examined the rainfall rates averaged over tracked hail and severe hail storms. The average rainfall in the cell also is shown to peak shortly after the initiation of hail.

Figure 16 showed that there is a 10-minute difference in rainfall onset before a HE between north and south. In the south, rainfall around a HE (both before and after a HE) occurs in a grid cell for a longer time, when compared to the north. The earlier onset of rainfall can likely contribute overall higher rainfall amounts before and after a HE in the south. The longer time of rainfall per grid cell can also be interpreted as a slower propagation of the storm.

However, from Figure 15 it is known that the previously described streak in Ticino is the only area in the south, where there is on average more rainfall before a HE. It is hard to determine to what extent the streak contributes to the earlier onset of rainfall before a HE.

Panziera et al. (2015) showed that the extreme rainfall in the Lago Maggiore region comes about from the contributions of multiple rain storms. One would expect that contributions of consecutive storms are visible as "bumps" in the rainfall rate time series, as the rain storms pass over the same grid cell. A clear signature of the consecutive rain storms is not visible in the rainfall distribution around a HE in Figure 16. Importantly, although the presence of the small "bumps" can suggest rainfall contributions from additional rain storms to the rainfall accumulation, the reverse argument cannot be made. That is, although in the average rainfall rate distribution only one rainfall peak is visible, that does not exclude the possibility that in some cases there are additional rain storms before and after the HE. The additional rainfall contributions are likely not visible in Figure 16 because they do not have a periodic occurrence. That is, the preceding or following rain storms do not occur at the same time distance and over the same areas. Additionally, it is likely that in Figure 16 these "bumps" are not visible because of the large amount of data that is averaged over (73 000 HEs).

Finally, I suggest that it is likely that both of the possible contributors (earlier onset and the streak) are to some extent adding to the higher cumulative rainfall before a HE in the south when

compared to the north.

There are other alternative potential reasons for the earlier onset of rainfall before the initiation of hail in the south. For example, it is possible that the cloud microphysics that leads to the creation of rain and hail are different. Panziera et al. (2015) concluded that the heavy rainfall in the streak is created by low-level coalescence, which occurs lower in the atmosphere than the creation of hail. This could lead to increased rainfall before a HE, as hail will have a longer fall time. Unfortunately, it is not possible to explore this only by using CPC and POH data and looking at a three-dimensional radar reflectivity would be required.

5.2.3 Monthly and hourly differences

Motivated by the literature that explores monthly and diurnal cycles of hail and rainfall occurrence (Section 1.2), this part of the analysis discusses the results on the differences of cumulative rainfall around a HE between convective season months and hours of the HE occurrence (Section 4.2.3).

Importantly, more data is needed to draw robust conclusions or identify drivers of intraseasonal or diurnal variability, as in some hours of the day or months of the year very few data points are available for the analysis.

Monthly differences Figure 17 shows that in the spring and autumn months, there are fewer HEs than in the summer. This is in agreement with NCCS (2021) and Nisi et al. (2016) which show the frequency of hail peaks in June and July.

The summer months do not show the highest median values of accumulated rainfall before and after a HE. In Figure 17 (c) it is visible that, especially in the south, the rainfall values in September are higher before and after hail, in comparison to other months. Indeed, Panziera et al. (2018) and Isotta et al. (2014) report the highest average of 24-hour rainfall seasonal maxima in Ticino to occur in the autumn. Additionally, there are fewer HEs in September due to lower temperatures but rainfall rates are high (Panziera et al., 2018). The combination of fewer hail episodes and more intense rainfall can likely explain the high September values.

In essence, from the analysis of the 2021 convective season, there is no easily identifiable pattern and associated process that can explain the intraseasonal variability of HE-related rainfall. However, it seems likely that in the south the increased cumulative rainfall in September is associated with an increased rainfall rate and frequency.

Hourly differences In the north, the cumulative rainfall after a HE peaks at 1800 UTC. This peak is in line with the previous observations that hail and rainfall in the northern part of the study area has a strong diurnal cycle with peaks from early afternoon to early evening (Nisi et al., 2016). Given that, it is known from section 5.2.2, that the largest contributions to the cumulative rainfall occur close to and during the HE itself, it is not surprising that the peak cumulative rainfall occurs in the late afternoon, when the rainfall tends to be the most frequent and intense north of the Alps (Barton et al., 2020; Panziera et al., 2018).

In the south, there is a high intra-hourly and inter-hourly variability in the rainfall before a HE, with multiple peaks (Figure 18 (c)). It is hard to interpret these peaks due to multiple

contributing factors to the cumulative rainfall, for example, the propagation speed of the hail storm and contributions of additional convective cells.

A very interesting feature of the diurnal cumulative rainfall differences in the south is that the cumulative rainfall values before and after a HE are not significantly different between 2100-0100 UTC (Figure 18 (c)). To explore the hours when the difference between the cumulative rainfall before and after a HE is not significantly different, Figure 19 shows the rainfall rate distribution around the HE that occurs in the specified hours. Although the main rainfall rate peak is located around the HE, before the HE, smaller "bumps" of the 75% quantile are visible. These "bumps" visually suggest that between 2100-0100 UTC in the south there are considerable contributions from the preceding rain storms to the cumulative rainfall before a HE. Although the "bumps" indicate only a small increase in the median rainfall rate, it has to be stressed that the time series in Figure 19 is averaged over 2000 different HEs. In each of the HEs, the preceding rain storm can occur at a different time and, therefore, not show large average values at a certain time step before or after a HE.

The results further agree with the proposed idea that the larger variability of cumulative rainfall in the south arises from there being a weak convective diurnal cycle south of the Alps (Barton et al., 2020).

5.2.4 The effect of estimated hail size

Next, the possible link between the cumulative rainfall around a HE and the MESHS size class is investigated. The results in Figure 20 show a decreasing amount of cumulative rainfall before a HE with increasing hail size class (Figure 20).

Nisi et al. (2018) results showed that the larger the MESHS size, the more explosive development the storm tends to have (shorter distance and time duration between storm path initiation and hail streak start). The higher explosivity can likely explain the decreased rainfall before a HE which is shown in Figure 20. Similarly, the slight decrease also can be linked to the increased storm velocity for severe hail storms when compared to regular hail storms (Feldmann et al., 2023). Feldmann et al. (2023) found a 5-8 km/h translational speed difference between hail storms and severe hail storms, which are associated with MESHS $\geq$ 4 cm. This likely could be enough of a translational speed difference to contribute to the small observed differences in the rainfall before a HE between the MESHS size category groups.

Nisi et al. (2020) found that for hail storms vertically integrated liquid (VIL) values are higher than for rain storms. The higher VIL is associated with the strength and persistence of the updraft that transports moisture upwards. If we consider this, then one would assume that the larger hail size groups should result in stronger rainfall, as the VIL is higher from stronger and more prolonged updrafts. However, the results here show a decrease, rather than an increase in accumulated rainfall with increasing hail size group. This can likely be attributed to the increased storm movement speed with increased storm severity, reported by Feldmann et al. (2023).

To summarise, it is likely that hail storms with larger hail stones are associated with more intense rainfall. However, this is counteracted by increased storm explosivity and propagation speed, therefore, the cumulative rainfall per area is actually slightly decreased with more severe

hail storms. These results highlight how likely important the storm propagation speed is for the cumulative rainfall in the area.

5.2.5 The effect of fronts

Synoptic forcing (Schemm et al., 2016) and thermal flows associated with orography (Nisi et al., 2020) are the main hail storm initiation mechanisms in Switzerland. Up to 45% of hail episodes in Switzerland occur in frontal or pre-frontal regions (Schemm et al., 2016). Therefore, it is of interest to investigate, how the presence of a front impacts the rainfall around a HE. In general, it is expected that HEs associated with fronts will experience higher accumulated rainfall after the HE, due to the presence of stratiform rainfall. However, the results (Section 4.2.5) are not in agreement with such a hypothesis.

Figure 21 shows that in the north the presence of a front leads to a lower accumulated rainfall before and after a HE. In the south, the opposite is true, whereby the presence of a front leads to higher median cumulative rainfall amounts around a HE. To explain the observed differences in the cumulative rainfall amounts north and south, a hypothesis is proposed and explained below.

Fronts tend to be associated with a stronger wind shear and speed (Schemm et al., 2016). On a first-order basis, the propagation speed of a convective cell is largely dependent on the mid-level wind speed (Panziera et al., 2015). Therefore, it is likely that the HEs that are associated with a front have faster propagation speed due to stronger environmental wind and, therefore, accumulate less rainfall over one area.

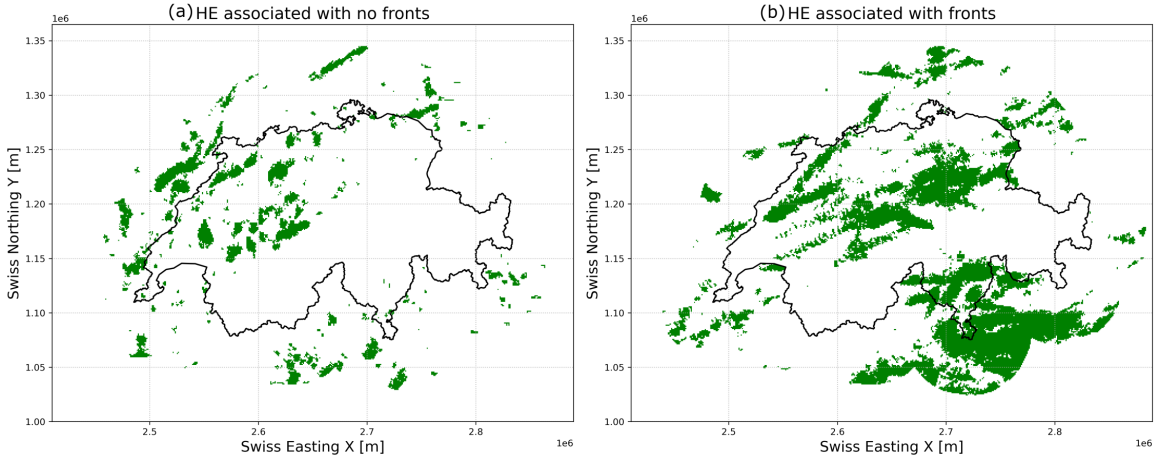

Figure 25: Hail episode footprints on days when (a) no front was present, (b) a front was present over the study area. (b) includes only dates from 15th July to 30th September because if all days of the convective season are plotted then there is too much overlap and the individual hail streaks are not visible.

To investigate this theory, Figure 25 shows the HE areas on the days when (a) no fronts are present and (b) when fronts are present over the study area. (a) shows more round hail streak patches, while (b) is characterised by elongated hail streaks. Although not quantified, by visually analysing Figure 25, it can be suggested that the lower overall rainfall is associated with a faster movement of the hail storm, as indicated by elongated streaks rather than patches. Indeed, Nisi et al. (2018) lagrangian hail storm study also proposes that the hail storms that occur in frontal

and pre-frontal environments last longer and cover larger distances due to higher wind shear and steering winds.

Figure 22 shows the distribution of rainfall rate for HEs without (a) and with (b) a front present and further strengthens the argument. For the HEs which are associated with a front, the rainfall over a grid cell lasts for a shorter time, when compared to the HEs that occur when no front is present. This is in agreement with the proposed idea that hail cells that are associated with a front move faster due to a stronger steering flow.

In the southern area, HEs that occur when a front is present are associated with higher cumulative rainfall around a HE (Figure 21). Visually, Figure 25 (b) shows similar but shorter streaks in the southern part of the study area, when compared to the north.

One likely reason for these results is that hail storms in the south get orographically blocked because of the flow that is induced by the front. Most commonly on hail days, fronts enter the study region from the west (Nisi et al., 2016; Schemm et al., 2016). When these fronts encounter the Alps, the flow south of the Alps is deformed and a south-to-southeasterly flow towards the Alps is induced (Panziera et al., 2015). The advected airmass is usually unstable, warm and moist and originates from the Po Valley (Panziera et al., 2015). The unstable flow encounters the Alps, is lifted and creates convective cells to release the instability, but the propagation of the cells is limited due to the orography, especially if the wind direction is uniform throughout the atmospheric column (i.e. towards the Alps). On the northern side, fronts are associated with the western flow that moves the convective cells across the northern areas where they are not trapped by the orography. Indeed, Feldmann et al. (2023) found lower wind speeds associated with hail and severe hail storms in the south, when compared to the north.

Also, Aregger (2021) climatology shows that southern Prealps are characterised by a lower number of long-track, long-duration storms and an increased number of stationary storms when compared to other regions in Switzerland.

In essence, when a front approaches from the west, in the south the hail storms get orographically trapped, while in the north they are not restricted by orography. In the case of hail occurring without a front present, it is shown how even a lower average rainfall rate can contribute to higher cumulative rainfall values by persisting over an area for a longer period of time.

5.2.6 Comparison to the case study

The cumulative rainfall before and after the HE on 28 June 2021 will now be compared to the results from the analysis of the convective season. This is done to put into context the sequence of events that occurred in the case study day.

First, the differences in the cumulative rainfall amounts before and after a HE on the case study day agree with the seasonal analysis. That is, it is not unusual that significantly more cumulative rainfall occurs after the HE rather than before.

However, the results of the case study disagree with the convective season analysis by showing an overall lower cumulative rainfall amount after the HE in the southern study area when compared to the north. This discrepancy between the case study and the season analysis is likely attributed to the northern area experiencing more severe and larger storms than the south on 28 June 2021.

On the case study day a front was present in the study area. Given the large area that the storms covered on the day (Kopp et al., 2022), the presence of a front is not surprising, as it likely contributed to the storm propagation.

Figure 12 suggests an additional storm contribution to the cumulative rainfall after the HE in the north on the case study day. With the current results, it is challenging to conclude whether the occurrence of an additional rain storm after the HE is unusual in the north.

Interestingly, the streak north of the Lago Maggiore that is discussed in subsection 5.2.1 was observed also in the case study rain episodes (Figure 8). However, on the specific day, no hail occurred in that region, therefore, the extreme rainfall registered did not contribute to the compound event.

In summary, overall there is a good agreement between the case study day cumulative rainfall and the results of the seasonal analysis.

5.2.7 Sensitivity analysis

The sensitivity and robustness of the results of the convective season analysis is discussed here. More specifically, the effects of the chosen study area on the results. Additionally, the differences between the cumulative rainfall from the start of a HE and the cumulative rainfall from the end of a HE are adressed.

Swiss territory versus the study area It is possible that the differences between the north and south cumulative rainfall arise from the fact that, in the study area, the southern area is dominated by the region outside the Swiss borders (Figure 7). This can likely have an impact because CPC only integrates rain gauges from within the Swiss borders. Therefore, the CPC data for the area between the border of Switzerland and the edge of the study area (Figure 7) is mostly radar measurements. In other words, the rainfall estimate "contamination" and higher rainfall values should be reported in the area between the Swiss border and the study area. Therefore, comparing the results from within Switzerland to the whole study area can indicate whether the results still hold if only the Swiss territory is taken into account.

Figure 23 compares the rainfall before and after a HE for the grid cells within Swiss borders and across the whole study area. One would expect that the whole study area should show higher median and extreme values, as the recorded reflectivity would represent the hail reflectivity and not all data points are "ground truth" corrected. This indeed in the case for the results in the northern stdy area (Figure 23 (b)).

However, in the south (c), interestingly, the values within the whole study area are significantly smaller than only within the Swiss borders. Although an unexpected result, it is likely because of the previously discussed ellipsoid streak in Ticino that likely dominates the values (Figure 15, 13 (a-c)).

In summary, although there still is a large uncertainty involved in this study, this section suggests that the higher rainfall values in the southern part of the study area do not arise from the CPC data that is not corrected by rain gauges.

Cumulative rainfall from the start of a HE versus from the end of a HE All figures in this thesis include the cumulative rainfall estimate from the start of a HE and an estimate for rainfall from the end of the HE. What are the differences and how do the two compare?

For testing the sensitivity of the results, it is important to check whether the results still hold if only the rainfall after the HE is considered. It is possible that no or light rainfall occurred during a HE but the hailstone reflectivity has artificially increased the rainfall estimate. By excluding the rainfall during a HE, only the rainfall that is not (likely) affected by the hail signal is summed up. Although the 6-hour rainfall after the end of the HE might be lower than the area actually experienced, by considering this value, the anomalously high rainfall estimates that occur during a HE are eliminated.

Figure 13 shows that the median of the cumulative rainfall value after the start of the HE is higher than the median of the cumulative rainfall value after the end of the HE. However, the cumulative rainfall value after the end of the HE is significantly higher than the median cumulative rainfall before a HE. A similar result can be seen in the majority of box plots presented in this thesis.

Assuming that the rainfall estimates are not positively skewed due to the presence of hail stones, the difference between the two cumulative rainfall values after the HE is expected because it is common for hail and rainfall to occur at the same time (Goodman et al., 1988). Moreover, the heaviest rainfall occurs shortly after hail initiation (Feldmann et al., 2023) (Figure 16). Therefore, excluding the heavy rainfall that falls during the HE, contributes to the difference in cumulative rainfalls after HE.

In summary, the cumulative rainfall amount after the start of the HE is likely an overestimation and the cumulative rainfall amount after the end of the HE is likely an underestimation of the rainfall that a specific area experienced. Both 6-hour cumulative rainfall amounts after a HE are associated with some uncertainty. However, regardless of which one is considered, it is in almost all cases significantly higher than the cumulative rainfall before a HE.

5.3 Limitations

All of the results in this thesis must be interpreted with caution because of the variety of uncertainties associated with the data. In the following section, the limitations of each of the data types and methods are discussed.

Rainfall "contamination" One of the main limitations of the study is the fact that both rainfall (CPC) and hail (POH, MESHS) data sets are derived from the same reflectivity signal. This introduces large uncertainty about rainfall estimates in cases when hail is present in the cloud, as the hail signal can increase the rainfall estimate. To reduce the possibility that the results of the thesis are heavily impacted by the rainfall signal contamination at the time of hail, I primarily focused on the 6-hour cumulative rainfall amounts. In my opinion, these results are likely less impacted by the contamination error than, for example, the comparison of time steps between hail and rainfall.

Another aim of this thesis was to explore whether using only POH and CPC data is enough

to confidently assess the co-occurrence of hail and rainfall. After having completed the analysis, I would suggest in the future exploring the co-occurrence of hail and rainfall with additional data sets, ideally the ones that provide the "ground truth" information, as that would greatly increase the confidence in the results. Further suggestions and an outlook for the field can be found in subsection 6.3. This limitation can be reduced by developing more ground-truth measurement stations for both hail and rainfall, so the radar estimates could be validated and improved upon.

Lack of validation Further, a major limitation is the nature of radar hail estimates. Although using POH data as a proxy for hail occurrence is common in the literature (e.g., Nisi et al. (2016), Schemm et al. (2016)), the main limitation of this technique, however, is its verification. Due to the fact that there is no extensive ground hail measurement network, it is hard to validate radar hail estimates. It is possible to use insurance claim data or crowd-sourced data for validation. However, both of these sources come with additional uncertainties, as they, for example, are mainly available for more populated areas, rather than areas with more hail.

Time and space displacement of hail Although POH algorithm estimates the probability of hail reaching the ground, it does not account for the time that the "observed" hail needs to reach the ground. This means that there likely is a time lag between the observed hail in the storm and it reaching the ground. Additionally, due to the fact that hail falls from 7-5 km height and strong storms are associated with wind shear, there can be a displacement in where the hail is observed in the cloud and where it actually reaches the ground. The likely spatial and temporal displacement of hail has to be acknowledged when working with POH in high resolution, like in this thesis. However, this is a hard problem to tackle, as hail occurrence is highly localised and averaging over the neighbouring grid cells can introduce uncertainty.

Considering this, it is possible that the hail that is "observed" at one 5-minute time step in the mid-troposphere but arrives on the ground in the following 5-minute interval. This raises questions about the certainty of the recorded end of a hail episode, as it might actually be later when we account for the fall time. However, it is hard to estimate how big of an impact this introduces. Additionally, the fall time of hail stones is a very complicated variable to adjust for as it is impacted by the size, shape, density, updraft speed, wind shear, melting and other factors, therefore not easy to account for.

CPC outside of Swiss territory The CPC data set collects the rain gauge data from within Switzerland, so the values outside the borders are mostly just radar estimates. The kriging between rain gauge measurements and radar estimates stretches a few tens of kilometres outside of the Swiss border and gradually fades into the radar estimate. The rainfall signal "contamination" by the hail signal in the locations far away from the Swiss territory is more prominent, as it is not corrected by rating gauges anymore. In subsection 5.2.7 we explored the effect of this and concluded that the main regional differences cannot be attributed to this problem. However, it is important to bear in mind the possible bias in the results.

Limited analysed time The results in this thesis are limited by the fact that only one convective season and one case study are analysed. Due to the fact that hail and rainfall occurrence has interannual variability, the results represent only a "snapshot" of the climatological values of rainfall before and after hail. For example, in the convective season analysis there are areas with no records on the cumulative rainfall around a HE, as hail did not occur everywhere in 2021 convective season.

"Fishbone patterns" In Figure 10 and 9 a "fishbone pattern" in the radar reflectivity measurements is visible. The patterns come about due to the interaction between the time it takes the radar to make one scan (2.5 minutes) and the fast-propagating convective system (Lukach et al., 2017). That means that the radar is not able to capture a "snapshot" of the current reflectivity field, but rather captures the propagation of the system.

The observation of the "fishbone pattern" in the co-occurrence sequence results suggests that comparing 5-minute CPC and POH time steps might not be suitable for reliable analysis of hail and rainfall occurrence times, as the measurement path seems to have an impact on the results. Lukach et al. (2017) concluded that using advection correction in the POH data post-processing greatly reduces the effect.

6 Conclusions and outlook

The aim of this thesis was to investigate the co-occurrence of hail and rainfall in Switzerland, motivated by the potentially large damages to infrastructure in the case of a compound event. The thesis presents a case study of 28 June 2021 and an analysis of the 2021 convective season. 5-minute radar data products, namely, POH and CPC, were used for hail and rainfall estimations. Additionally, one of the aims of this master's thesis was to explore the uncertainties associated with using POH and CPC data to explore hail and rainfall in high spatiotemporal resolution. The information about the Eulerian rainfall occurrence in relation to hail provides new insights into the characteristics of hailstorms and gives useful information for insurance companies.

6.1 Case study

In the first part of the thesis, a case study of 28 June 2021 was conducted to analyse a hail-rainfall compound event and explore ways of quantifying the co-occurrence of hail and rainfall. The specific date was chosen because it was reported as one of the costliest hail-related episodes in recent decades (Kopp et al., 2022). On 28 June 2021, hail and rainfall co-occurred in large areas of Switzerland, including densely populated cities like Luzern and Zurich. Storm path over cities and the longevity of the storms were likely some of the main contributors to the extensive damages. An additional factor that likely contributed to the large damages, is that a hail and extreme rainfall co-occurred.

The case study results show that:

1. Large areas of the study area experienced both hail and extreme rainfall on the study day, thereby creating a large co-occurrence area. 85% of the area where hail occurred also experienced extreme amounts of rainfall (Figure 8, section 4.1.1, 5.1.1).

2. The sequence of hail and rainfall occurrence depends on the threshold of the rainfall rate chosen (Figure 9, 10, Section 4.1.2, 5.1.2). In general, at least light rain (with a rain rate as low as 0.08 mm/h) is recorded before or within 10 minutes of hail over the whole co-occurrence area. In 88% of the co-occurrence area, hail and extreme rainfall (24 mm/h rainfall rate) occurred within the same 10-minute interval (Figure 9), thereby creating a compound event.

3. It is hard to precisely answer the question "What was the time difference between rainfall and hail occurrence?" due to the uncertainties in the data. First, a rainfall threshold must be chosen which can be a subjective choice due to the lack of agreed on definitions. Second, when occurrence times are compared, a "fishbone pattern" is visible in the results, which indicates that comparing 5-minute CPC and POH time steps might not be suitable for reliable analysis of hail and rainfall occurrence times, as the measurement path seems to have an impact on the results (Section 4.1.2).

4. There was significantly less rainfall in the 6 hours before the HE (median 0.5 mm), when compared to the 6-hour cumulative rainfall after (median value 21.6 mm after the start of a HE and 14.8 mm after the end of the HE). The difference between pre- and post-HE rainfall is the largest north of the Alps (the difference between the median before a HE and after the start of a HE is 22.2 mm). Southern parts show a more equal distribution of rainfall

before and after HE per 1 km^2 (8.5 mm difference between medians). The cumulative rainfall amounts around a HE can be linked by the rainfall rate distribution in northern and southern regions (Figure 12).

5. The rainfall rate time series show that the main contribution to the accumulated rainfall occurs closely around the HE and it is different between northern and southern study areas. In the south, on average there was an earlier onset of the rainfall before a HE, but in the north the rainfall lasted longer after the HE (Figure 12, Section 4.1.3). The longer post-HE rainfall in the north can be attributed to the occurrence of a mesoscale convective system (Kopp et al., 2022) or following additional rain storms. The rainfall following a HE is important, because Hohl et al. (2002) hypothesised that the contributions to the damages of multiple convective cells are not proportionally additive but the loss increases dramatically with each consecutive cell crossing the same area.

6.2 Convective season analysis

To better quantify the average rainfall amounts before and after hail episodes, an analysis of the cumulative rainfall (6 hours before a HE, 6 hours after the start of a HE and 6 hours after the end of a HE) was carried out for the whole convective season of 2021. This also allows us to put into wider context the results from the case study and see whether the previously discussed difference between rainfall before and after a HE is a common occurrence or a special feature of the case study day that contributed to the large flood damages.

The analysis of the 2021 convective season led to the following results and conclusions:

1. The cumulative amount of rainfall in the 6 hours before a HE is significantly smaller than in the 6 hours following the HE (Figure 13). It can likely be explained by (1) hail and rainfall being created in the same updraft, but hail stones falling out earlier and at higher velocities, therefore, reaching the ground before the rainfall and (2) the life cycle of hail storms where the hail producing cell weakens with time and later is able to produce only raindrops.

2. In all of the presented results, the median 6-hour cumulative rainfall amount after the start of the HE is higher than the median 6-hour cumulative rainfall amount after the end of the HE. However, the cumulative rainfall after the end of the HE is overall still significantly higher than the cumulative rainfall value before a HE. This indicates that by disregarding the rainfall at the time of the largest associated uncertainties (time of the HE), the results are still valid.

3. In the 2021 convective season, the areas that experience the highest hail frequency (Figure 13 (e)) are not the same areas where the highest cumulative rainfall values before and after the hail (Figure 13 (a,b)). That is, hail occurrence frequency is not linked to the rainfall associated with the hail episode.

4. The amount of rainfall before and after a HE per grid cell is not uniform over the study area and there are differences between northern and southern Switzerland (Figure 13, 14, Section 5.2.1). Very few HEs occurred over the main Alpine chain. South of the Alps in general

show larger cumulative rainfall values and a greater spread of these values than in the north (Figure 14).

5. There is a distinct streak in Figure 13 (a-c) southern areas near the Lago Maggiore that show higher pre- and post-HE cumulative rainfall values. A similar feature was explored in Panziera et al. (2015) where they looked into the precipitation episodes that cause flash floods in the region. The elliptical streak likely comes about due to echo training of convective cells. In addition, this thesis shows that one of the consecutive convective cells that form the streak can produce hail, not just rainfall.

6. The rainfall rate distribution (Figure 16, Section 5.2.2) shows that on average, the largest contributions to the cumulative rainfall around a HE occurs close to the HE and the rainfall rate peaks 5 minutes after the HE start. On average, a grid cell in the south, experiences a longer rainfall around a HE (earlier onset and later end), when compared to the north. The longer accumulation time and higher peak rainfall rate (56 mm/h in the south and 45 mm/h in the north) likely explain the overall higher cumulative rainfall values and more equal rainfall distribution around a HE. Although it is known that locally more than one rain storm contributes to the high accumulated rainfall (Panziera et al., 2015), these contributions were not visible in the median rainfall rate distribution in Figure 16 likely due to averaging over a large sample of HEs and a non-periodic occurrence of the additional rain storms.

7. During the night-time convection in the southern study area (2100 - 0100 UTC) the rain accumulation before and after a hail episode is not significantly different (Figure 18). It is suggested that this arises from the active night-time convection characteristic in southern Switzerland (Panziera et al., 2015; Barton et al., 2020). In the northern study area, regardless of the time of HE occurrence, the rainfall before the HE is significantly lower than the rainfall after the HE, except at 0400 and 0800 UTC when very few data points are available. For more robust results of the seasonal and diurnal differences of cumulative rainfall around a HE, more data is needed.

8. There is a decrease in the cumulative rainfall amount before a HE for increasing hail size groups (Figure 20). This can likely be attributed to the higher explosivity and storm propagation speed of more intense storms that counteract the proposed higher vertically integrated liquid values. I suggest that these results highlight how important the storm propagation speed is for the cumulative rainfall in the area.

9. The presence of fronts impacts the cumulative rainfall around a hail episode (Section 5.2.5). Fronts that are located less than approximately 200 km from the study area are considered. In the north, overall less rainfall is associated with HEs which occur when a front is present. In the south, the presence of a front leads to a higher rainfall before a HE than without a front. By looking at the footprints of HEs not associated with a front (Figure 25 (a)) and HEs associated with a front (Figure 25 (b)), it is suggested that the higher winds, which are associated with fronts, lead to a faster propagation speed of the convective cells. In the north, the storms typically propagate east to west and do not encounter large orography. In the

south, however, the dominant wind direction induced by fronts leads to the convective storm propagation into the main Alpine chain and slowing down or becoming stationary there.

10. Multiple results in the thesis point towards the south having larger contributions to the cumulative rainfall around a HE of preceding or following rain storms. For example, the rainfall streak in Ticino (Section 5.2.1) and the equal distribution of rainfall around a HE at night (Section 18). Given the results in this thesis, I would suggest that the contribution from additional storms to the cumulative rainfall around a HE in the north is smaller than in the south.

11. The cumulative rainfall around a HE on the case study day was compared to the results of the convective season analysis. There is an overall agreement between the results, as both results show that more rainfall tends to occur during and after a HE, when compared to the cumulative rainfall before a HE. However, on the case study day, the median cumulative rainfall was lower in the southern part of the study area, which is not the case in the seasonal analysis. This is explained by a particularly severe storm north of the Alps on the case study day.

12. To investigate whether the choice of the study area influences the results (because CPC is corrected with rain gauges only within the Swiss territory), the results were compared within Switzerland to the chosen study area (Figure 23, Section 4.2.6). Due to the areas outside of Switzerland having large contributions to the southern study area, there was an expectation that higher cumulative rainfall values arise from a larger proportion of radar-only data. In the northern part, the results showed a smaller rainfall accumulations within Swiss borders. However, in the south, the average rainfall values within the Swiss border were actually higher than the average through the southern study area. This can likely be linked to the large contributions to the average rainfall accumulations from the streak in Ticino, which is located within Swiss borders.

6.3 Outlook

Due to the large uncertainties surrounding the hail estimates and their relevance in everyday life, I think that this is a developing and important field in meteorology. Moreover, given the chaotic nature of hail, it is important but very challenging to predict how hail storms and hail and rainfall co-occurrence will change under climate change. Further details on the challenges are in detail discussed in Raupach et al. (2021).

I believe that the field of hail research will strongly benefit from an automatic hail detection network, like the one mentioned in Kopp et al. (2023) to validate and improve the current hail-estimation algorithms. A well-established data set of "ground-truth" hail measurements would help with not only hail estimates, but also improve the rainfall "contamination" correction possibilities.

There are multiple possible avenues for future research to further explore hail and rainfall co-occurrence:

1. Performing the convective season analysis for more than one year to increase the data points and capture the interannual variability of the phenomenon.

2. The topic of co-occurrence can be very interesting to explore from a Lagrangian perspective, similar to what is done is Nisi et al. (2018) and Feldmann et al. (2023), but focusing more on the rainfall and hail occurrence along the storm track. Object-driven studies can give insights into typical storm characteristics, repetitive patterns of storm initiation and precipitation which could likely improve the forecasting of severe storms.

3. Investigating the co-occurrence of hail and rainfall in other areas where hail occurs often and where hail research is carried out, like Australia or the US. It would be interesting and relevant to see whether in other areas there also is a difference between rainfall before and after a HE.

4. Test how the propagation speed of a storm affects the cumulative rainfall per area, related to MESHS hail size groups and the effect of fronts.

5. The proposed mechanisms that might lead to more rainfall after the hail episode are (1) hail and rainfall being created in the same updraft, but hail stones falling out earlier and at higher velocities, therefore, reaching the ground before the rainfall and (2) the life cycle of hail storms where the hail producing cell weakens with time and later is able to produce only raindrops. It would be worthwhile to test what contributions each of the proposed mechanisms has.

6. In the case study there were areas that experienced a HE but not extreme rainfall and they were located on the edges of hail occurrence. Explore whether this comes from storm dynamics or is a radar signal peculiarity.

7. Compare POH and the hydrometeor classification data. This would allow us to explore the impacts of spatial and temporal displacement of hail and rainfall estimates that are discussed in the subsection 5.3 on Limitations.

8. Use the thunderstorm radar tracking (TRT) data set (Hering et al., 2004) to investigate the contributions of preceding or following convective storms to the cumulative rainfall amount around a HE.

A Appendix

	Whole study area			North			South		
Test between the 6-hour cumulative rainfall **before** a HE and 6-hour cumulative rainfall **after the start of the HE**		**Wilcoxon Statistic**	**p-value**		**Wilcoxon Statistic**	**p-value**		**Wilcoxon Statistic**	**p-value**
	Case study	460887	0	Case study	80449	0	Case study	76638	0
	Seasonal analysis	125937735	0	Seasonal analysis	7373554	0	Seasonal analysis	47632298	0
Test between the 6-hour cumulative rainfall **before** a HE and 6-hour cumulative rainfall **after the end of the HE**		**Wilcoxon Statistic**	**p-value**		**Wilcoxon Statistic**	**p-value**		**Wilcoxon Statistic**	**p-value**
	Case study	1229674	0	Case study	172853	0	Case study	224147	0.003
	Seasonal analysis	285572754	0	Seasonal analysis	26070891	0	Seasonal analysis	103338676	0

Figure 26: P-values and test statistics of the Wilcoxon Signed-Ranks significance tests between (1) the cumulative rainfall before a HE and the cumulative rainfall after the start of a HE, (2) the cumulative rainfall before a HE and the cumulative rainfall after the end of a HE. P-value of "0" is in places, where the reported p-value was smaller than 10^{-10}. Results for the box plots in Figures 11, 13, 14 are shown.

	Whole study area			North			South		
Test between the 6-hour cumulative rainfall **before** a HE and 6-hour cumulative rainfall **after the start of the HE**	**Front group**	**Wilcoxon Statistic**	**p-value**	**Front group**	**Wilcoxon Statistic**	**p-value**	**Front group**	**Wilcoxon Statistic**	**p-value**
	No front	286870	0	No front	118523	0	No front	1120	0
	Front	3707321.5	0	Front	5631848	0	Front	97029432	0
Test between the 6-hour cumulative rainfall **before** a HE and 6-hour cumulative rainfall **after the end of the HE**	**Front group**	**Wilcoxon Statistic**	**p-value**	**Front group**	**Wilcoxon Statistic**	**p-value**	**Front group**	**Wilcoxon Statistic**	**p-value**
	No front	1417722	0	No front	781698	0	No front	87804	0
	Front	244695875	0	Front	17266728	0	Front	991721	0

Figure 27: Same as for Figure 26 but for box plots in Figure 21.

Test between the 6-hour cumulative rainfall **before** a HE and 6-hour cumulative rainfall **after the start of the HE**			Test between the 6-hour cumulative rainfall **before** a HE and 6-hour cumulative rainfall **after the end of the HE**		
MESHS size class	**Wilcoxon Statistic**	**p-value**	**MESHS size class**	**Wilcoxon Statistic**	**p-value**
0-2 cm	50497771	0	0-2 cm	100150113	0
2-4 cm	10369098	0	2-4 cm	30436465	0
4-6 cm	482088	0	4-6 cm	1443472	0
>6 cm	1570	0	>6 cm	7020	0

Figure 30: Same as Figure 26 but for box plots in Figure 20.

Whole study area

Test between the 6-hour cumulative rainfall **before** a HE and 6-hour cumulative rainfall **after the start of the HE**

	Month	Wilcoxon Statistic	p-value
0	2021-04	0.0	2.500000e-01
1	2021-05	0.0	1.730181e-48
2	2021-06	5631295.0	0.000000e+00
3	2021-07	49047508.0	0.000000e+00
4	2021-08	728541.0	0.000000e+00
5	2021-09	1340.0	2.613365e-72

Test between the 6-hour cumulative rainfall **before** a HE and 6-hour cumulative rainfall **after the end of the HE**

	Month	Wilcoxon Statistic	p-value
0	2021-04	0.0	2.500000e-01
1	2021-05	11.0	1.943162e-48
2	2021-06	20225427.0	0.000000e+00
3	2021-07	98347558.0	0.000000e+00
4	2021-08	2638119.0	0.000000e+00
5	2021-09	3477.0	1.888944e-66

North

	Month	Wilcoxon Statistic	p-value
0	2021-04	0.0	2.500000e-01
1	2021-05	0.0	7.547498e-11
2	2021-06	9831376.0	0.000000e+00
3	2021-07	1278149.0	0.000000e+00
4	2021-08	605132.0	0.000000e+00
5	2021-09	0.0	2.029468e-22

	Month	Wilcoxon Statistic	p-value
0	2021-04	0.0	2.500000e-01
1	2021-05	0.0	7.547498e-11
2	2021-06	9831376.0	0.000000e+00
3	2021-07	1278149.0	0.000000e+00
4	2021-08	605132.0	0.000000e+00
5	2021-09	0.0	2.029468e-22

South

	Month	Wilcoxon Statistic	p-value
0	2021-05	0.0	2.542378e-39
1	2021-06	383856.0	0.000000e+00
2	2021-07	31392565.0	0.000000e+00
3	2021-08	246307.0	0.000000e+00
4	2021-09	1241.0	1.081304e-50

	Month	Wilcoxon Statistic	p-value
0	2021-05	9.0	2.861605e-39
1	2021-06	1155987.0	1.253576e-148
2	2021-07	64249805.0	0.000000e+00
3	2021-08	729281.0	0.000000e+00
4	2021-09	2852.0	9.258664e-45

Figure 28: Same as Figure 26 but for box plots in Figure 17. Here the calculated p-values are displayed fully.

Test between the 6-hour cumulative rainfall **before** a HE and 6-hour cumulative rainfall **after the start of the HE**

Whole study area

	Hour	Wilcoxon Statistic	p-value
0	0	12952.0	3.182146e-42
1	1	14054.0	2.154422e-11
2	2	1780.0	3.076231e-44
3	3	253.0	5.526164e-64
4	4	465.0	1.587661e-30
5	5	387.0	2.952870e-48
6	6	11807.0	3.459167e-156
7	7	121353.0	5.974309e-96
8	8	330224.0	1.613909e-03
9	9	102160.0	4.421895e-178
10	10	7013.0	0.000000e+00
11	11	84322.0	0.000000e+00
12	12	171277.0	0.000000e+00
13	13	480138.0	0.000000e+00
14	14	1759971.0	0.000000e+00
15	15	4819510.0	0.000000e+00
16	16	1235764.0	0.000000e+00
17	17	293753.0	0.000000e+00
18	18	205863.0	0.000000e+00
19	19	53121.0	0.000000e+00
20	20	35238.0	0.000000e+00
21	21	218221.0	3.612405e-155
22	22	62676.0	4.609821e-137
23	23	9835.0	4.943768e-54

North

	Hour	Wilcoxon Statistic	p-value
0	0	0.0	2.236324e-54
1	1	0.0	4.597822e-24
2	2	0.0	1.743790e-16
3	3	0.0	3.992170e-19
4	4	0.0	5.000000e-01
5	5	0.0	2.665141e-18
6	6	0.0	8.493989e-31
7	7	0.0	3.906250e-03
8	8	0.0	5.000000e-01
9	9	3.0	1.904118e-30
10	10	311.0	3.126238e-123
11	11	10007.0	4.202119e-238
12	12	4890.0	0.000000e+00
13	13	309.0	0.000000e+00
14	14	58467.0	0.000000e+00
15	15	176408.0	0.000000e+00
16	16	333466.0	0.000000e+00
17	17	131841.0	0.000000e+00
18	18	72708.0	0.000000e+00
19	19	13557.0	1.621013e-179
20	20	1881.0	5.775197e-220
21	21	18425.0	1.204989e-110
22	22	2289.0	3.882968e-99
23	23	3.0	1.039735e-44

South

	Hour	Wilcoxon Statistic	p-value
0	0	3519.0	1.897328e-01
1	1	8037.0	9.793148e-01
2	2	1354.0	4.534421e-29
3	3	251.0	2.442892e-46
4	4	459.0	3.313060e-30
5	5	249.0	9.347016e-32
6	6	9825.0	2.496175e-127
7	7	120486.0	1.282461e-94
8	8	329564.0	1.834634e-03
9	9	89959.0	5.165789e-151
10	10	2198.0	5.058107e-203
11	11	26294.0	2.682808e-187
12	12	78083.0	0.000000e+00
13	13	214627.0	0.000000e+00
14	14	755426.0	0.000000e+00
15	15	1567999.0	1.290007e-185
16	16	233965.0	0.000000e+00
17	17	28962.0	7.941703e-235
18	18	28724.0	5.134344e-109
19	19	12037.0	1.819830e-232
20	20	17888.0	1.567628e-202
21	21	99410.0	1.599317e-50
22	22	31252.0	5.247271e-40
23	23	8136.0	1.193622e-03

Test between the 6-hour cumulative rainfall **before** a HE and 6-hour cumulative rainfall **after the end of the HE**

	Hour	Wilcoxon Statistic	p-value
0	0	14981.0	6.080270e-38
1	1	18517.0	8.272570e-05
2	2	7259.0	3.070599e-25
3	3	3120.0	1.064395e-54
4	4	643.0	2.146948e-29
5	5	2800.0	2.585960e-38
6	6	92078.0	1.481682e-74
7	7	232536.0	8.613118e-33
8	8	318287.0	3.621798e-05
9	9	168606.0	7.214166e-135
10	10	49029.0	1.273229e-295
11	11	364787.0	4.074433e-303
12	12	532669.0	0.000000e+00
13	13	1667396.0	0.000000e+00
14	14	5557744.0	0.000000e+00
15	15	7779776.0	0.000000e+00
16	16	3908056.0	0.000000e+00
17	17	920159.0	0.000000e+00
18	18	428507.0	0.000000e+00
19	19	161757.0	0.000000e+00
20	20	213976.0	0.000000e+00
21	21	565755.0	4.897581e-26
22	22	181834.0	2.136213e-51
23	23	23492.0	1.860339e-27

	Hour	Wilcoxon Statistic	p-value
0	0	11.0	2.479056e-54
1	1	9.0	5.613036e-24
2	2	0.0	1.743790e-16
3	3	0.0	3.992170e-19
4	4	0.0	5.000000e-01
5	5	2.0	2.829514e-18
6	6	415.0	8.283024e-28
7	7	0.0	3.906250e-03
8	8	0.0	5.000000e-01
9	9	26.0	2.827491e-30
10	10	869.0	2.927712e-122
11	11	53033.0	8.432894e-203
12	12	24116.0	0.000000e+00
13	13	5015.0	0.000000e+00
14	14	234874.0	0.000000e+00
15	15	753306.0	0.000000e+00
16	16	1312581.0	0.000000e+00
17	17	377070.0	0.000000e+00
18	18	147145.0	0.000000e+00
19	19	26881.0	1.258739e-165
20	20	23029.0	4.667342e-200
21	21	71387.0	4.399121e-49
22	22	11123.0	6.220784e-82
23	23	78.0	2.455706e-44

	Hour	Wilcoxon Statistic	p-value
0	0	4005.0	8.871078e-01
1	1	5181.0	3.475650e-05
2	2	5160.0	2.675965e-12
3	3	3039.0	2.272613e-34
4	4	635.0	4.464142e-29
5	5	1986.0	2.292498e-21
6	6	73798.0	4.867537e-52
7	7	230792.0	6.912202e-32
8	8	316680.0	3.007739e-05
9	9	152666.0	7.261470e-107
10	10	19447.0	1.781131e-185
11	11	122940.0	3.409750e-107
12	12	240343.0	2.771801e-231
13	13	720416.0	2.799830e-254
14	14	2219264.0	2.090166e-205
15	15	2340469.0	3.825103e-67
16	16	650609.0	3.435188e-171
17	17	104721.0	9.316363e-179
18	18	62045.0	2.118556e-71
19	19	54220.0	1.719399e-197
20	20	81176.0	1.510629e-147
21	21	214738.0	1.884923e-01
22	22	77225.0	5.239605e-02
23	23	6477.0	2.811988e-07

Figure 29: Same as Figure 26 but for box plots in Figure 18. Here the calculated p-values are displayed fully.

	Whole study area			North			South		
Test between the 6-hour cumulative rainfall **before** a HE and 6-hour cumulative rainfall **after the start of the HE**	**Area**	**Wilcoxon Statistic**	**p-value**	**Area**	**Wilcoxon Statistic**	**p-value**	**Area**	**Wilcoxon Statistic**	**p-value**
	Swiss borders	20495280	0	Swiss borders	2145851	0	Swiss borders	2326789	0
	Study area	125937735	0	Study area	7373554	0	Study area	47632298	0
Test between the 6-hour cumulative rainfall **before** a HE and 6-hour cumulative rainfall **after the end of the HE**	**Area**	**Wilcoxon Statistic**	**p-value**	**Area**	**Wilcoxon Statistic**	**p-value**	**Area**	**Wilcoxon Statistic**	**p-value**
	Swiss borders	33751248	0	Swiss borders	6297704	0	Swiss borders	3325189	0
	Study area	285572754	0	Study area	26070891	0	Study area	103338676	0

Figure 31: Same as Figure 26 but for box plots in Figure 23.

Bibliography

Allen, J. T., Giammanco, I. M., Kumjian, M. R., Jurgen Punge, H., Zhang, Q., Groenemeijer, P., Kunz, M., and Ortega, K. (2020). Understanding hail in the earth system. *Reviews of Geophysics*, 58(1):e2019RG000665.

Aregger, M. P. (2021). Stationary and slow-moving convection over Switzerland: a 14-year radar-based climatology. Master's thesis, University of Bern.

Barras, H., Hering, A., Martynov, A., Noti, P., Germann, U., and Martius, O. (2019). Experiences with more than 50,000 crowdsourced hail reports in switzerland. *Bulletin of the American Meteorological Society*, 100(8):1429–1440.

Barton, Y., Sideris, I. V., Raupach, T. H., Gabella, M., Germann, U., and Martius, O. (2020). A multi-year assessment of sub-hourly gridded precipitation for switzerland based on a blended radar—rain-gauge dataset. *International Journal of Climatology*, 40(12):5208–5222.

Besic, N., Figueras i Ventura, J., Grazioli, J., Gabella, M., Germann, U., and Berne, A. (2016). Hydrometeor classification through statistical clustering of polarimetric radar measurements: A semi-supervised approach. *Atmospheric Measurement Techniques*, 9(9):4425–4445.

Delobbe, L. and Holleman, I. (2006). Uncertainties in radar echo top heights used for hail detection. *Meteorological Applications*, 13(4):361–374.

Feldmann, M., Germann, U., Gabella, M., and Berne, A. (2021). A characterisation of Alpine mesocyclone occurrence. *Weather and Climate Dynamics*, 2(4):1225–1244.

Feldmann, M., Hering, A., Gabella, M., and Berne, A. (2023). Hailstorms and rainstorms versus supercells—a regional analysis of convective storm types in the Alpine region. *npj Climate and Atmospheric Science*, 6(1):19.

Foote, B., Krauss, T., and Makitov, V. (2005). Hail metrics using conventional radar. *85th AMS Annual Meeting, American Meteorological Society - Combined Preprints*.

Germann, U., Boscacci, M., Gabella, M., and Sartori, M. (2015). Peak performance: Radar design for prediction in the Swiss Alps. *Meteorological Technology International*, 4:42–45.

Germann, U., Galli, G., Boscacci, M., and Bolliger, M. (2006). Radar precipitation measurement in a mountainous region. *Quarterly Journal of the Royal Meteorological Society*, 132:1669– 1692.

Goodman, S. J., Buechler, D. E., Wright, P. D., and Rust, W. D. (1988). Lightning and precipitation history of a microburst-producing storm. *Geophysical Research Letters*, 15(11):1185–1188.

Grahame, N., Riddaway, B., Eadie, A., Hall, B., and McCallum, E. (2009). Exceptional hailstorm hits Ottery St Mary on 30 October 2008. *Weather*, 64(10):255–263.

Hering, A., Morel, C., Galli, G., Sénési, S., Ambrosetti, P., and Boscacci, M. (2004). Nowcasting thunderstorms in the Alpine region using a radar based adaptive thresholding scheme. In *Proceedings of 3rd European Conference Radar in Meteorology and Hydrology (ERAD), 6–10 September 2004, Visby, Sweden*, pages 1–6.

Hohl, R., Schiesser, H. H., and Aller, D. (2002). Hailfall: the relationship between radar-derived hail kinetic energy and hail damage to buildings. *Atmospheric Research*, 63(3-4):177–207.

Houze Jr, R. A. (2004). Mesoscale convective systems. *Reviews of Geophysics*, 42(4).

Isotta, F. A., Frei, C., Weilguni, V., Perčec Tadić, M., Lassegues, P., Rudolf, B., Pavan, V., Cacciamani, C., Antolini, G., and Ratto, S. M. (2014). The climate of daily precipitation in the Alps: development and analysis of a high-resolution grid dataset from pan-Alpine rain-gauge data. *International Journal of Climatology*, 34(5):1657–1675.

Jenkner, J., Sprenger, M., Schwenk, I., Schwierz, C., Dierer, S., and Leuenberger, D. (2010). Detection and climatology of fronts in a high-resolution model reanalysis over the Alps. *Meteorological Applications*, 17(1):1–18.

Joe, P., Burgess, D., Potts, R., Keenan, T., Stumpf, G., and Treloar, A. (2004). The S2K severe weather detection algorithms and their performance. *Weather and Forecasting*, 19(1):43–63.

Joss, J., Schädler, B., Galli, G., Cavalli, R., Boscacci, M., Held, E., Della Bruna, G., Kappenberger, G., Nespor, V., and Spiess, R. (1998). *Operational use of radar for precipitation measurements in Switzerland*. vdf Hochschulverl. an der ETH Zürich.

Kopp, J., Manzato, A., Hering, A., Germann, U., and Martius, O. (2023). How observations from automatic hail sensors in Switzerland shed light on local hailfall duration and compare with hailpad measurements. *Atmospheric Measurement Techniques*, 16(14):3487–3503.

Kopp, J., Schroer, K., Schwierz, C., Hering, A., Germann, U., and Martius, O. (2022). The summer 2021 Switzerland hailstorms: weather situation, major impacts, and unique observational data. *Weather*, 99(99).

Kunz, M. and Kugel, P. I. (2015). Detection of hail signatures from single-polarization C-band radar reflectivity. *Atmospheric Research*, 153:565–577.

Lukach, M., Foresti, L., Giot, O., and Delobbe, L. (2017). Estimating the occurrence and severity of hail based on 10 years of observations from weather radar in Belgium. *Meteorological Applications*, 24(2):250–259.

McGill, R., Tukey, J. W., and Larsen, W. A. (1978). Variations of box plots. *The American Statistician*, 32(1):12–16.

MeteoSwiss (2023). Hail climatology. `https://www.meteoswiss.admin.ch/climate/the-climate-of-switzerland/hail-climatology.html`. Accessed: 2023-08-20.

NCCS (2021). Hail Climate Switzerland – National hail hazard maps. https://www.nccs.admin.ch/nccs/en/home/the-nccs/priority-themes/hail-climate-switzerland.html. (Accessed: 2023-06-06).

Nisi, L., Hering, A., Germann, U., and Martius, O. (2018). A 15-year hail streak climatology for the Alpine region. *Quarterly Journal of the Royal Meteorological Society*, 144(714):1429–1449.

Nisi, L., Hering, A., Germann, U., Schroeer, K., Barras, H., Kunz, M., and Martius, O. (2020). Hailstorms in the Alpine region: Diurnal cycle, 4d-characteristics, and the nowcasting potential of lightning properties. *Quarterly Journal of the Royal Meteorological Society*, 146(733):4170–4194.

Nisi, L., Martius, O., Hering, A., Kunz, M., and Germann, U. (2016). Spatial and temporal distribution of hailstorms in the Alpine region: a long-term, high resolution, radar-based analysis. *Quarterly Journal of the Royal Meteorological Society*, 142(697):1590–1604.

Panziera, L., Gabella, M., Germann, U., and Martius, O. (2018). A 12-year radar-based climatology of daily and sub-daily extreme precipitation over the Swiss Alps. *International Journal of Climatology*, 38(10):3749–3769.

Panziera, L., James, C., and Germann, U. (2015). Mesoscale organization and structure of orographic precipitation producing flash floods in the Lago Maggiore region. *Quarterly Journal of the Royal Meteorological Society*, 141(686):224–248.

Raupach, T. H., Martius, O., Allen, J. T., Kunz, M., Lasher-Trapp, S., Mohr, S., Rasmussen, K. L., Trapp, R. J., and Zhang, Q. (2021). The effects of climate change on hailstorms. *Nature Reviews Earth & Environment*, 2(3):213–226.

Ridder, N. N., Pitman, A. J., Westra, S., Ukkola, A., Do, H. X., Bador, M., Hirsch, A. L., Evans, J. P., Di Luca, A., and Zscheischler, J. (2020). Global hotspots for the occurrence of compound events. *Nature Communications*, 11(1):5956.

Sánchez, J., López, L., García-Ortega, E., and Gil, B. (2013). Nowcasting of kinetic energy of hail precipitation using radar. *Atmospheric Research*, 123:48–60.

Schemm, S., Nisi, L., Martinov, A., Leuenberger, D., and Martius, O. (2016). On the link between cold fronts and hail in Switzerland. *Atmospheric Science Letters*, 17(5):315–325.

Schumacher, R. S. and Johnson, R. H. (2005). Organization and environmental properties of extreme-rain-producing mesoscale convective systems. *Monthly Weather Review*, 133(4):961–976.

Schuster, S., Blong, R., Leigh, R., and McAneney, K. (2005). Characteristics of the 14 April 1999 Sydney hailstorm based on ground observations, weather radar, insurance data and emergency calls. *Natural Hazards and Earth System Sciences*, 5(5):613–620.

Sideris, I. V., Gabella, M., Erdin, R., and Germann, U. (2014). Real-time radar–rain-gauge merging using spatio-temporal co-kriging with external drift in the alpine terrain of Switzerland. *Quarterly Journal of the Royal Meteorological Society*, 140(680):1097–1111.

Treloar, A. (1998). Vertically integrated radar reflectivity as an indicator of hail size in the greater Sydney region of Australia. *Preprints, 19th Conference on Severe Local Storms, Minneapolis, MN, American Meteorological Society*, pages 48—-51.

Waldvogel, A., Federer, B., and Grimm, P. (1979). Criteria for the detection of hail cells. *Journal of Applied Meteorology and Climatology*, 18(12):1521–1525.

Wetter3.de (2023). UKMET Analyse-Archiv. `https://www.wetter3.de/archiv_ukmet_dt.html`. Accessed: 2023-08-20.

Widmann, M. and Schär, C. (1997). A principal component and long-term trend analysis of daily precipitation in Switzerland. *International Journal of Climatology: A Journal of the Royal Meteorological Society*, 17(12):1333–1356.

Wieringa, J. and Holleman, I. (2006). If cannons cannot fight hail, what else? *Meteorologische Zeitschrift*, 15(6):659–670.

Wilcoxon, F. (1945). Individual comparisons by ranking methods. *Biometrics Bulletin*, 1(6):80–83.

Woolson, R. F. (2007). Wilcoxon signed-rank test. *Wiley Encyclopedia of Clinical Trials*, pages 1–3.

Acknowledgements

I want to thank my supervisor Prof Dr Olivia Romppainen-Martius, co-supervisor Dr Cornelia Schwierz and my advisors Martin Aregger and Lena Wilhelm, for supporting me in the project. Their help and insightful suggestions have greatly improved this thesis's quality and direction.

I am also grateful for the support and the good vibes that my coursemates and friends have provided throughout the year.

Declaration of consent

on the basis of Article 30 of the RSL Phil.-nat. 18

Name/First Name: Stella Bērziņa

Registration Number: 21116207

Study program: Masters of Climate Science

Bachelor ☐ Master ☑ Dissertation ☐

Title of the thesis: Co-occurrence of hail and rainfall

Supervisor: Prof. Dr. O. Romppainen-Martius

I declare herewith that this thesis is my own work and that I have not used any sources other than those stated. I have indicated the adoption of quotations as well as thoughts taken from other authors as such in the thesis. I am aware that the Senate pursuant to Article 36 paragraph 1 litera r of the University Act of 5 September, 1996 is authorized to revoke the title awarded on the basis of this thesis.

For the purposes of evaluation and verification of compliance with the declaration of originality and the regulations governing plagiarism, I hereby grant the University of Bern the right to process my personal data and to perform the acts of use this requires, in particular, to reproduce the written thesis and to store it permanently in a database, and to use said database, or to make said database available, to enable comparison with future theses submitted by others.

Bern, 27 June 2023

Place/Date

Signature